OPTICAL COHERENCE GRATINGS AND LATTICES AND THEIR PROPAGATION PROPERTIES

by

Liyuan Ma

Submitted in partial fulfillment of the
requirements for the degree of
Master of Applied Science

at

Dalhousie University
Halifax, Nova Scotia
April 2015

For my parents

Table of Contents

List of Figures

Abstract

Partially coherent sources have been widely used in speckle-free imaging, distortionless information transfer and optical communications in free space. In this thesis, we introduce a novel class of partially coherent sources, the so-called optical coherence gratings/lattices and study their propagation properties in free space. The novel sources are constructed using the recently developed complex Gaussian representation of statistical pulses and beams. All novel sources generate either pulses with statistically stationary or beams with statistically homogeneous coherence properties in the source plane. Furthermore, the new class of sources shows periodic temporal or spatial coherence properties. We explore paraxial propagation of the beams generated by novel sources in free space. We give evidence of a novel phenomenon of periodicity reciprocity between the source intensity and coherence properties. We expect the new phenomenon to find applications to free-space optical communications.

List of Abbreviations and Symbols Used

Abbreviation	Description
GSM	Gaussian Schell-model
TGSM	Twisted Gaussian Schell-model
OCL	Optical coherence lattices
CGR	Complex Gaussian Representation
RMS	Root-Mean-Square

Symbols	Description
Re	Real part
Im	Imaginary part
c	Speed of light in free-space
τ	Time difference
k	Wave number
ω	Angular frequency
∇	Laplace operator
δ	Delta operator
γ	Complex degree of coherence
μ	Spectral degree of coherence
$\widetilde{\omega}$	Mean frequency of light
v	Visibility of the interference fringes
J	Radiant intensity
I	Light intensity
S	Spectral density
Γ	Mutual coherence function
W	Cross-spectral density function
t_s	Time delay
ω_s	Carrier frequency shift
A	Amplitude

Symbols	Description
t_*	Width of the pulse
σ_I	RMS width of the source
$\sigma(z)$	RMS width of the beam
v_n	Energy distribution
$R(z)$	Radius of the curvature
z_R	Rayleigh length
$\Delta(z)$	Expansion coefficient

Acknowledgements

Foremost, I owe my deepest gratitude to my supervisor Dr. Sergey Ponomarenko for his guidance, patience, immense knowledge and support during my MASc study. Without his help, it is impossible for me to finish the research and to write this thesis.

Besides my supervisor, I would like to thank the rest of my committee: Dr. Zhizhang Chen and Dr. William Philips for reading the thesis, and their useful comments and recommendations.

Furthermore, I would also like to thank to all the colleagues in my group for their generous attitude and friendly behavior.

Finally, I would like to thank my parents: Yonglin Ma and Wenqiao Zhang for giving birth to me at the first place, raising me up and supporting me all the time.

Chapter 1

Introduction

In 1960, the first functioning laser [1, 2] was deployed at Hughes Research Laboratories. Since then, laser technology has developed quickly. Lasers are highly coherent sources that have wide usage in laser biology, atomic physics, optical communications and related fields. However, because these sources may cause speckle phenomena in imaging [3, 4] and can be easily affected by turbulence during propagation [5, 6], partially coherent sources are now being designed.

In 1978, E. Wolf discussed the relation between the state of coherence of the source and the intensity distribution of the light it generates. He pointed out that sources of different states of coherence can generate the same intensity distribution in the far zone [7, 8]. At the same time, he proved that certain kinds of partially coherent sources may generate light that has the same intensity distribution as the laser source in the far zone [7, 9, 10]. Later, E. Wolf showed that under very general conditions, the cross-spectral density of a statistically stationary source of any state of coherence can be expressed as a superposition of coherent modes [13, 14, 15]. This new theory opened a new perspective for analyzing partially coherent sources. Inspired by this theory, the study of partially coherent sources has attracted a lot of attention to date[11, 12].

The Gaussian-Schell Model (GSM) sources are useful for modeling highly directional partially coherent beams. In 1978, Wolf predicted that under suitable circumstances, this model would produce the same far-field optical intensity distribution as does a fully coherent laser [7, 9, 10]. The GSM sources attracted particular interest because the sources and fields they generate can be readily realized in a laboratory [16, 17]. In 1993, Simon introduced a new type of partially coherent sources termed Twisted Gaussian-Shell model (TGSM) sources. The twist phase of the new source does not affect the intensity and coherence distribution in any transverse plane. However, the upper bound of the strength of the twist phase captures the subtle nature

of this phase and distinguishes it from the other familiar phase curvature [18, 19].

In 1987, Gori evaluated the modes for a Schell-model planar source whose optical intensity distribution is an arbitrary circularly symmetric function and complex degree of coherence is a zero order Bessel function. This source is called a Bessel-correlated source and, like a coherent Bessel source, it can generate beams propagating over a long distance with little spreading in free space [20].

In 2001, Ponomarenko introduced a new class of partially coherent sources with a separable phase. This phase acquires a vortex structure on paraxial propagation in free space. Similar to the GSM source, this partially coherent source shows shape invariance on its paraxial propagation. However, unlike the GSM source, the spectral degree of coherence of this partially coherent source is independent of the relative orientation of the pair of points in the transverse plane [21].

The sources mentioned here cover all classes of partially coherent sources with their cross-spectral densities known in a closed form. Most have been widely used in speckle-free image formation, distortion-less information transfer, and optical communications in free space. Partially coherent sources have proved able to reduce the system bit error rate due to the radiance scintillations in the receiver focal plane arising due to the atmospheric turbulence [22]. In addition, some non-shape-invariant partially coherent beams such as cos-Gaussian and cosh-Gaussian beams were shown to form stable structures during short-distance propagation in the atmosphere [23]. Thus, partially coherent beams have been employed in optical communications in atmospheric systems.

In this thesis, a class of partially coherent temporal/spatial sources, the so-called optical coherence gratings/lattices is introduced and its propagation properties in free space are examined. This new class of partially coherent sources has a Gaussian intensity profile and is statistically stationary/homogeneous with periodic degree of coherence. Further, this new class of sources have an interesting property, periodicity reciprocity which can be used in robust free-space optical communications.

The remainder of the thesis consists of 5 chapters. Chapter 2 discusses the basic concept of coherence and optical coherence in space-time and space-frequency domains. It introduces Young′s interference experiment (used in studying coherence

properties), discusses the representation of coherent modes, and reviews the properties of the GSM source as an example of a partially coherent source. Chapter 3 reviews partial coherence of non-stationary fields, demonstrating temporal coherence properties with the Michelson interferometer and introducing a complex Gaussian representation of statistical pulses. Chapter 4 describes the new class of partially coherent sources with Gaussian intensity profiles and periodic coherence properties. This chapter also presents the radiant intensity and complex degree of coherence of this new source in temporal and spatial cases. Chapter 5 examines free-space paraxial propagation of the fields generated by the source proposed in Chapter 4 and demonstrates a novel phenomenon of the periodicity reciprocity between their intensity profile and degree of coherence. It also explores the possibility of employing novel sources in free space optical communications. Chapter 6 summarizes the thesis and discusses potential future research directions.

Chapter 2

Statistically Stationary Sources in Space-Time and Space-Frequency Domain

2.1 Young's interference experiment

When two or more light waves combine, they form a pattern of light and dark regions. This happens because the combined light fields have constructively or destructively interfered. However, when we study the interference fringes, we find that some light sources easily produce sharp interference fringes while others appear to have difficulty producing them. Optical coherence can be used to describe the ability of light waves to produce interference fringes. Generally, when two optical fields combine and produce no interference fringes, they are said to be uncorrelated, whereas if they produce clear interference fringes, they are said to be perfectly correlated. Furthermore when the two light waves produce interference fringes between these two conditions, they are said to be partially correlated. Based on different aspects, optical coherence can be divided into spatial coherence and temporal coherence. Spatial coherence measures the correlation of waves at pairs points on their propagation or the correlation of a wave with a spatially shifted version of itself, while temporal coherence shows the correlation of a wave at different times at the same position or the correlation of the wave with the time-delayed version of itself.

Optical coherence is a physical concept that can be studied experimentally. Most manifestations of coherence between optical fields are provided by the phenomena of interference. Therefore, we can obtain information about source coherence with experimental observation of interference phenomena. There are two famous experiments that highlight the two types of coherence. One is Young's interference experiment, and the other is the Michelson interference experiment. The first experiment describes spatial coherence, while the second one measures the ability of light to interfere with time delays which illustrates temporal coherence of light. In this chapter, we discuss

spatial coherence with Young's interference experiment, which deals with the ability of a light field to interfere with a spatially-shifted version of itself.

Young's double-slit interference experiment is named after its inventor, Thomas Young. It plays an important role in both classical [24, 25] and quantum optics [26, 27, 68] and connects many basic concepts in optical physics. A simple schematics of the experiment is shown in Fig. 2.1. In the experiment, a light source is positioned behind a screen containing two narrow pinholes. As light emerges from the pinholes Q_1 and Q_2 in plane A, the waves overlap and interference fringes are formed on the observation screen B located some distance away from the pinholes. Usually, we can obtain a pattern of bright or dark lines on the observation screen where light waves from the pinholes interfere, constructively or destructively.

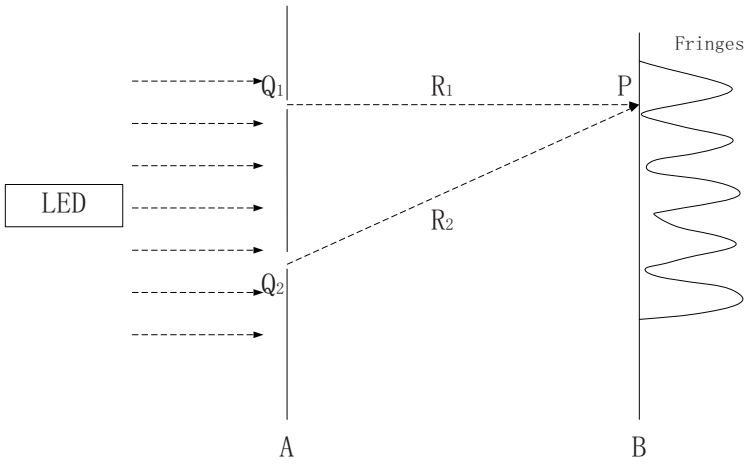

Figure 2.1: Illustrating Young's interference experiment.

The experiment demonstrates that some kinds of sources can produce sharp interference fringes while other sources can hardly generate any interference fringes. The ability of the sources to produce interference fringes is quantified by its degree of coherence. For example, sunlight which is a low spatial coherence source generates dim interference fringes on the observation screen; while a highly coherent laser source can produce sharp interference fringes. Hence, the visibility of interference fringes is closely connected to the degree of coherence of the source.

In the experiment, the light waves emerge from the pinholes and travel to the observation screen. Assuming the fields at the pinholes Q_1 and Q_2 can be expressed

as $V(Q_1, t)$ and $V(Q_2, t)$, light reaches the point P on the observation screen after

$$t_1 = \frac{R_1}{c}, t_2 = \frac{R_2}{c}, \tag{2.1}$$

respectively, where c is the speed of the light in free space, and $R_i (i = 1, 2)$ is the distance from the pinhole to the observation screen.

The field at point P is a superposition of two light waves traveling to the observation screen, which can be expressed as

$$V(P, t) = K_1 V(Q_1, t - t_1) + K_2 V(Q_2, t - t_2). \tag{2.2}$$

It is worth noting that fluctuations of the wave field are very rapid and cannot be measured directly. We can only measure average properties of the field. In this chapter, we consider only statistically stationary sources. Since the properties of statistically stationary sources depend only on the time difference τ ($\tau = t_2 - t_1$), the intensity of light at point P in this experiment can be expressed as $I(P) = \langle I(P, t) \rangle = \langle V^*(P, t) V(P, t) \rangle$ where the angle brackets denote ensemble averages. We then obtain [28]

$$I(P) = |K_1| I(Q_1) + |K_2| I(Q_2) + 2Re|K_1||K_2| \Gamma(Q_1, Q_2, t_1 - t_2), \tag{2.3}$$

where $I(Q_j) = \langle V^*(Q_j, t) V(Q_j, t) \rangle$ are averaged intensities of light at each pinhole and $K_j (j = 1, 2)$ is a diffraction parameter based on the Huygens-Fresnel principle [29]. The function

$$\Gamma(Q_1, Q_2, \tau) = \langle V^*(Q_1, t) V(Q_2, t + \tau) \rangle, \tag{2.4}$$

is known as the mutual coherence function of the field at two pinholes Q_1, Q_2.

In Eq.(2.3), the first two terms on the right-hand side represent the intensity of the fields at point P when only one pinhole is open. Hence, the first of these two terms can be written as

$$I(P) = I^{(1)}(P), \tag{2.5}$$

when the pinhole Q_2 is closed.

Similarly, if Q_1 is closed, the intensity at P is

$$I(P) = I^{(2)}(P). \tag{2.6}$$

When we combine Eq.(2.5) and Eq.(2.6) with Eq.(2.4), the intensity of light at point P can be rewritten as

$$I(P) = I^{(1)}(P) + I^{(2)}(P) + 2Re\sqrt{I^{(1)}}\sqrt{I^{(2)}}\gamma(Q_1, Q_2, t_1 - t_2). \tag{2.7}$$

Here

$$\gamma(Q_1, Q_2, \tau) = \frac{\Gamma(Q_1, Q_2, \tau)}{\sqrt{\Gamma(Q_1, Q_1, 0)}\sqrt{\Gamma(Q_2, Q_2, 0)}}. \tag{2.8}$$

The quantity γ is known as the complex degree of coherence, while Eq.(2.7) is the interference law for statistically stationary optical fields. It follows from Eq.(2.8) that the absolute value of γ is bounded by unity. For $|\gamma|$ is zero, the source is incoherent; for $|\gamma|$ is 1, the source is fully coherent; and for the other cases, the source is partially coherent.

Using the envelope representation of narrow-band signals [30], Eq.(2.8) can be represented in an alternative form

$$I(P) = I^{(1)}(P) + I^{(2)}(P) + 2\sqrt{I^{(1)}}\sqrt{I^{(2)}}|\gamma(Q_1, Q_2, \tau)|\cos[\alpha(Q_1, Q_2, \tau) - \delta], \tag{2.9}$$

where

$$\delta = \overline{\omega}\tau, \tag{2.10}$$

and $\overline{\omega}$ is a mean frequency of light.

For commonly occurring symmetric situations when $I^{(1)}(P) = I^{(2)}(P)$, the interference law Eq.(2.9) reduces to

$$I(P) = 2I^{(1)}(P)\left\{1 + |\gamma(Q_1, Q_2, \tau)|\cos[\alpha(Q_1, Q_2, \tau) - \delta]\right\}. \tag{2.11}$$

In physics, the visibility of interference fringes is defined as [28]

$$v(P) = \frac{I_{max}(P) - I_{min}(P)}{I_{max}(P) + I_{min}(P)}. \tag{2.12}$$

Here the maximum and minimum of the average intensity on the observation screen at point P are given by

$$I_{max}(P) = 2I^{(1)}(P)[1 + |\gamma(Q_1, Q_2, \tau)|], \tag{2.13}$$

and

$$I_{min}(P) = 2I^{(1)}(P)[1 - |\gamma(Q_1, Q_2, \tau)|]. \tag{2.14}$$

Substituting from Eq.(2.13), Eq.(2.14) into Eq.(2.12), gives us an interesting result:

$$v(P) = |\gamma(Q_1, Q_2, \tau)|. \tag{2.15}$$

This result relates the degree of coherence of the source to the visibility of interference fringes. Therefore the visibility of interference fringes is a direct measure of spatial coherence of the wave field. In Young's interference experiment, I_{max} and I_{min} are the intensity in the brightest and dimmest regions on the observation screen. If there are no fringes in the experiment, the light waves at the two pinholes are uncorrelated. If sharp fringes are generated on the observation screen, it means the light waves are highly correlated. In essence, Young's interference experiment provides a method to determine spatial coherence of the wave field by directly measuring the intensity of the fringe pattern.

2.2 The coherent mode representation in space-frequency domain

In section 2.1, coherence phenomena were described in terms of space-time correlation functions, namely the mutual coherence function $\Gamma(\mathbf{r_1}, \mathbf{r_2}, \tau)$, and the complex degree of coherence $\gamma(\mathbf{r_1}, \mathbf{r_2}, \tau)$. There is, however, an alternative description that describes coherence phenomena in the space-frequency domain. The Fourier representation does not exist for the sample functions of a stationary random process because the Fourier integral does not converge. Thanks to the Wiener-Khintchine theorem [14, 29, 31], for wide-sense-stationary random processes the spectral density and its autocorrelation function form a Fourier-transform pair. It then follows that the cross-spectral density function is a Fourier transform of the mutual coherence function.The new description has been proven to be very useful for providing solutions to numerous problems.

In the space-time domain, the mutual coherence function of a statistically stationary optical field is defined as

$$\Gamma(\mathbf{r_1}, \mathbf{r_2}, \tau) = \langle V^*(\mathbf{r_1}, t) V(\mathbf{r_2}, t+\tau) \rangle \,, \tag{2.16}$$

where $V(\mathbf{r}, t)$ is a fluctuating function of space and time .

According to the Wiener-Khintchine theorem [14], the cross-spectral density function is the Fourier transform of the mutual coherence function:

$$W(\mathbf{r_1}, \mathbf{r_2}, \omega) = \frac{1}{2\pi} \int_{-\infty}^{+\infty} \Gamma(\mathbf{r_1}, \mathbf{r_2}, \tau) e^{i\omega\tau} d\tau. \tag{2.17}$$

For special cases, when $\mathbf{r_1} = \mathbf{r_2} = \mathbf{r}$, the cross-spectral density function becomes the spectral density

$$S(\mathbf{r}, \omega) = W(\mathbf{r}, \mathbf{r}, \omega). \tag{2.18}$$

By definition, the spectral degree of coherence can be expressed as

$$\mu(\mathbf{r_1}, \mathbf{r_2}, \omega) = \frac{W(\mathbf{r_1}, \mathbf{r_2}, \omega)}{\sqrt{S(\mathbf{r_1}, \omega)}\sqrt{S(\mathbf{r_2}, \omega)}}. \tag{2.19}$$

It can be shown that the magnitude of spectral degree of coherence is between zero and one. When $|\mu| = 0$, the field is completely incoherent; when $|\mu| = 1$ the field is completely coherent; and when $0 < |\mu| < 1$, the field is partially coherent.

In the 1980s, E. Wolf proposed a new theory of partial coherence [14]. In his theory, he uses the Karhunen-Loeve expansion of a random process [32] to show that a statistically stationary optical field of any state of coherence can be represented as a superposition of coherent modes.

When we look back at the cross-spectral density function of Eq.(2.17), there are several useful properties. First, assuming the cross-spectral density is a continuous function of $\mathbf{r_1}$ and $\mathbf{r_2}$ in a certain domain D, $|W(\mathbf{r_1}, \mathbf{r_2}, \omega)|^2$ is necessarily bounded in D, i.e, [32]

$$\int\int_D |W(\mathbf{r_1}, \mathbf{r_2}, \omega)|^2 d\mathbf{r_1} d\mathbf{r_2} < \infty. \tag{2.20}$$

It means the cross-spectral density is a Hilbert-Schmidt Kernel.

Second, the mutual coherence function satisfies

$$\Gamma(\mathbf{r_2}, \mathbf{r_1}, \tau) = \Gamma^*(\mathbf{r_1}, \mathbf{r_2}, \tau) \tag{2.21}$$

implying that its Fourier transform function also follows

$$W(\mathbf{r_2}, \mathbf{r_1}, \tau) = W^*(\mathbf{r_1}, \mathbf{r_2}, \tau), \tag{2.22}$$

which is called a Hermitian symmetry.

In addition, it has been shown in Ref [32] that $W(\mathbf{r_1}, \mathbf{r_2}, \tau)$ is a nonnegative definite function in the sense that for any function $f(\mathbf{r})$

$$\int\int_D W(\mathbf{r_1}, \mathbf{r_2},\omega) f^*(\mathbf{r_1}) f(\mathbf{r_2}) d^3\mathbf{r_1} d^3\mathbf{r_2} \geq 0. \tag{2.23}$$

According to Mercer's theorem [14, 33, 34], any continuous, Hermitian, nonnegative definite Hilbert-Schmidt kernel can be expressed as

$$W(\mathbf{r_1}, \mathbf{r_2},\omega) = \sum_n \lambda_n(\omega) \phi_n^*(\mathbf{r_1},\omega) \phi_n(\mathbf{r_2}, \omega), \tag{2.24}$$

where$\{\lambda_n\}$ are the eigenvalues and $\{\phi_n\}$ are orthonormal eigenfunctions of the integral equation

$$\int W(\mathbf{r_1}, \mathbf{r_2},\omega) \phi_n(\mathbf{r_1}, \omega) d\mathbf{r_1} = \lambda_n(\omega) \phi_n(\mathbf{r_2},\omega), \tag{2.25}$$

with the integration extending over the source. Eq.(2.24) is known as the coherent-mode representation of the cross-spectral density [14]. This new expression plays a very important role in optics. It provides a new method to analyze generation, propagation and transformation of partially coherent light. Furthermore, it simplifies numerical computations in statistical optics.

2.3 Gaussian Schell-model sources

As mentioned in Chapter 1, in order to avoid speckle formation in optical imaging, partially coherent sources have been widely used in optics. Gaussian Schell-model source(GSM) presents a convenient generic model. The GSM sources give rise to exactly the same far-field optical intensity distributions as do fully coherent lasers but with reduced spatial coherence [9, 10]. At the same time, GSM are easy to generate in a laboratory which makes them particularly important in practice.

A planar secondary Gaussain Shell-model source is characterized by the property that its spectral degree of coherence μ depends on the difference of in-plane position vectors $\boldsymbol{\rho'} = \boldsymbol{\rho_2} - \boldsymbol{\rho_1}$ [35]. Both the spectral intensity distribution and the spectral degree of coherence are Gaussian. According to the definition, the cross-spectral density function of this kind of sources is

$$W^{(0)}(\boldsymbol{\rho'_1}, \boldsymbol{\rho'_2}, \omega) = \sqrt{S^{(0)}(\boldsymbol{\rho'_1}, \omega)} \sqrt{S^{(0)}(\boldsymbol{\rho'_2}, \boldsymbol{\rho})} \mu^{(0)}(\boldsymbol{\rho'_2} - \boldsymbol{\rho'_1}, \omega), \tag{2.26}$$

where $S^{(0)}$ is the spectral density of the source and μ represents the spectral degree of coherence of light vibrations at any pair of points in the source plane. Further, the spectral density and the degree of coherence have Gaussian profiles that can be expressed as

$$S^{(0)}(\boldsymbol{\rho}) = A\exp(-\boldsymbol{\rho}^2/2\sigma_s^2), \tag{2.27}$$

and

$$\mu^{(0)}(\boldsymbol{\rho'}) = \exp(-\boldsymbol{\rho'}^2/2\sigma_\mu^2), \tag{2.28}$$

respectively, where A, σ_s and σ_μ are the parameters that depend on the frequency of the source.

Consider a random wave-field generated by a partially coherent source. Its free-space propagation is governed by the homogeneous Helmholtz equation,

$$(\nabla^2 + k^2)V(R) = 0. \tag{2.29}$$

Let $V(R)$ be a monochromatic scalar wave field propagating in the positive z-direction. It can be represented as

$$V(R) = v(\boldsymbol{\rho}, z)\exp(ikz), \tag{2.30}$$

where $\boldsymbol{\rho} = (x, y)$ and k is the free-space wave number. In a transverse plane $z = constant$, the cross-spectral density function can be expressed as

$$W(\boldsymbol{\rho_1}, \boldsymbol{\rho_2}; z) = \langle v^*(\boldsymbol{\rho_1}, z)v(\boldsymbol{\rho_2}, z)\rangle\,, \tag{2.31}$$

where the phase factor $\exp(ikz)$ is canceled out because of the complex conjugation. For a beam-like field, $v(\boldsymbol{\rho}, z)$ is a slowly varying function of z.In the paraxial approximation, the term $\partial^2 v/\partial z^2$ in Eq.(2.29) can be neglected. Then one can readily show that $v(\boldsymbol{\rho}, z)$ obeys the so-called parabolic equation [29]

$$(\nabla_\rho^2 + 2ik\frac{\partial}{\partial z})v(\boldsymbol{\rho}, z) = 0. \tag{2.32}$$

Following the well-known solution to the parabolic equation [37], we can obtain

$$v(\boldsymbol{\rho}, z) = \frac{-ik}{2\pi z}\int\int_{-\infty}^{\infty} v(\boldsymbol{\rho'}, 0)\exp[ik(\boldsymbol{\rho} - \boldsymbol{\rho'})^2/2z]d\boldsymbol{\rho'}. \tag{2.33}$$

Here, $v(\boldsymbol{\rho}, 0)$ is the optical field in the source plane. It then follows at once from Eq.(2.33) and Eq.(2.31) that

$$\begin{aligned} W(\boldsymbol{\rho_1}, \boldsymbol{\rho_2}; z) = \left(\frac{k}{2\pi z}\right)^2 \int\int\int\int_{-\infty}^{\infty} W^{(0)}(\boldsymbol{\rho_1'}, \boldsymbol{\rho_2'}, \omega) \\ \times \exp\left\{-ik[[(\boldsymbol{\rho_1} - \boldsymbol{\rho_1'})^2 - (\boldsymbol{\rho_2} - \boldsymbol{\rho_2'})^2]/2z]\right\} d\boldsymbol{\rho_1'}d\boldsymbol{\rho_2'}. \end{aligned} \tag{2.34}$$

On substituting from Eq.(2.26)-(2.28) into Eq.(2.34), we can obtain after tedious but

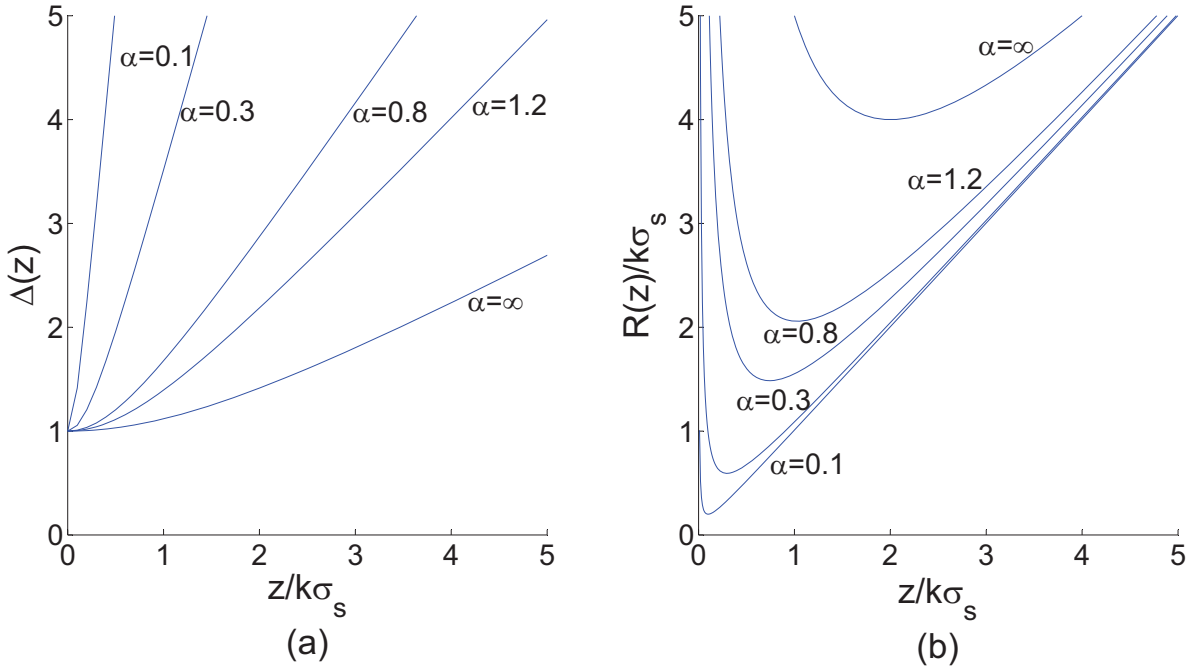

Figure 2.2: Behavior of (a) the expansion coefficient $\Delta(z)$ and (b) the radius of the curvature $R(z)$ of the Gaussian Schell-model beam.

straightforward algebra, the transverse cross-spectral density of GSM beam as [36]

$$W(\boldsymbol{\rho_1}, \boldsymbol{\rho_2}, ; z) = \frac{A}{[\Delta(z)]^2} \exp\left\{-\frac{(\boldsymbol{\rho_1}+\boldsymbol{\rho_2})^2}{8\sigma_s^2[\Delta(z)]^2}\right\} \times \exp\left\{-\frac{(\boldsymbol{\rho_1}-\boldsymbol{\rho_2})^2}{2\sigma_\mu^2[\Delta(z)]^2}\right\} \exp\left\{-i\frac{k(\boldsymbol{\rho_1^2}-\boldsymbol{\rho_2^2})}{2R(z)}\right\}, \tag{2.35}$$

where

$$\Delta(z) = \left[1 + (\frac{z}{k\sigma_s\sigma_t})^2\right]^{1/2}, \tag{2.36}$$

$$R(z) = z\left[1 + (\frac{k\sigma_s\sigma_t}{z})^2\right], \tag{2.37}$$

and

$$\frac{1}{\sigma_t^2} = \frac{1}{4\sigma_s^2} + \frac{1}{\sigma_\mu^2}. \tag{2.38}$$

The optical intensity in any transverse plane $z = const$ is given by

$$I(\boldsymbol{\rho}, z) = W(\boldsymbol{\rho}, \boldsymbol{\rho}, z) = \frac{A}{[\Delta(z)]^2} \exp\left\{-\frac{\boldsymbol{\rho}^2}{2\sigma_s^2[\Delta(z)]^2}\right\}. \tag{2.39}$$

The complex degree of coherence can then be expressed in the form

$$\mu(\boldsymbol{\rho_1}, \boldsymbol{\rho_2}, z) = \exp\left\{-\frac{(\boldsymbol{\rho_1} - \boldsymbol{\rho_2})^2}{2\sigma_\mu^2[\Delta(z)]^2}\right\} \exp\left\{-i\frac{k(\boldsymbol{\rho_1^2} - \boldsymbol{\rho_2^2})}{2R(z)}\right\}. \tag{2.40}$$

It has been shown elsewhere [38] that $w(z) = 2\sigma_I\Delta(z)$ and $R(z)$ are the beam width and the radius of wavefront curvature respectively which describe the evolution of the GSM beam. The ratio $\alpha = \sigma_\mu/\sigma_s$ is a measure of the degree of global coherence of light across the source plane $z = 0$. The case $\alpha \to \infty$ corresponds to a completely coherent GSM beam, while the case $\alpha \to 0$ represents a nearly incoherent GSM beam. The behavior of the beam width and the radius of curvature as a function of the dimensionless variable $z/k\sigma_s$ for several values of α is shown in Fig2.3.

It is seen in Fig. 2.3 that with a fixed value of σ_s, the beam width for any partially coherent GSM beam is larger than that for a fully coherent GSM beam. At the same time, the magnitude of the radius of curvature for a partially coherent GSM beam is always smaller than that for a fully coherent GSM beam.

Chapter 3

Coherence Properties of Non-Stationary Sources

3.1 Michelson interferometer and temporal coherence of pulse

In chapter 2, the theory of coherence for statistically stationary sources was discussed. A different situation exists when the source is non-stationary. At present, only a few studies have been carried out on coherence of non-stationary sources[39, 40, 41]. According to the second-order coherence theory of non-stationary sources, temporal coherence properties of pulse trains can be characterized by two-time mutual coherence function, defined as [42, 43]

$$\Gamma(\mathbf{r}; t_1, t_2) = \langle E^*(\mathbf{r}; t_1) E(\mathbf{r}; t_2) \rangle . \tag{3.1}$$

Usually, this is a 3×3 matrix function. However, it is sufficient to consider one component of the coherence matrix for linear polarized pulse. The optical intensity of the random field is defined as

$$I(\mathbf{r}; t) = \Gamma(\mathbf{r}; t, t) = \left\langle |E(\mathbf{r}; t)|^2 \right\rangle . \tag{3.2}$$

One can further introduce a normalized form of the mutual coherence function as

$$\gamma(\mathbf{r}; t_1, t_2) = \frac{\Gamma(\mathbf{r}; t_1, t_2)}{\sqrt{I(\mathbf{r}; t_1) I(\mathbf{r}; t_2)}}. \tag{3.3}$$

Here γ is known as the complex degree of coherence between field fluctuations at one point in space and two instants of time. It can be shown that $0 \leq |\gamma| \leq 1$. The lower limit indicates complete incoherence while the upper limit implies full coherence at the appropriate space-time points. When the intensity of two pulses are equal, the visibility of interference fringes equals to the absolute value of the complex degree of coherence. Inspired by this characteristic, Micheson's interferometer can be used to measure temporal coherence of pulse trains.

The Michelson interferometer is well-known for its use by Albert Michelson and Edward Morley in their famous 1887 Michelson-Morley experiment [44]. The configuration was to have detected Earth's motion through the supposed luminousness of

aether, which many physicists at that time believed was the medium through which light waves propagated. Nowadays, the Michelson interferometer is a standard tool for measuring temporal coherence of statistical sources. In analogy to spatial coherence, temporal coherence is a measure of average correlations between a wave amplitude and its replica delayed by τ. It entails wave correlations at a given point in space at different instance of time. However, in the case of pulses, the time delay introduced here means relative temporal intensities of the two interfering copies of the pulse change with time, and the visibility of interference fringes is time-dependent. It means the time-integrated visibility is not a true measure of temporal coherence for pulse trains. Recently, it has been shown that the standard Michelson interferometer is adequate to estimate temporal coherence of pulse trains [45].

Fig.3.1 is the setup of an equal-path-length Michelson interferometer which is employed to measure temporal coherence of pulses. It consists of two plane mirrors A and B, a beam-splitter and an observation screen. Both plane mirrors are tilted at a small angle $\pm\theta$ as shown in the figure. Spatial interference fringes form on the observation screen.

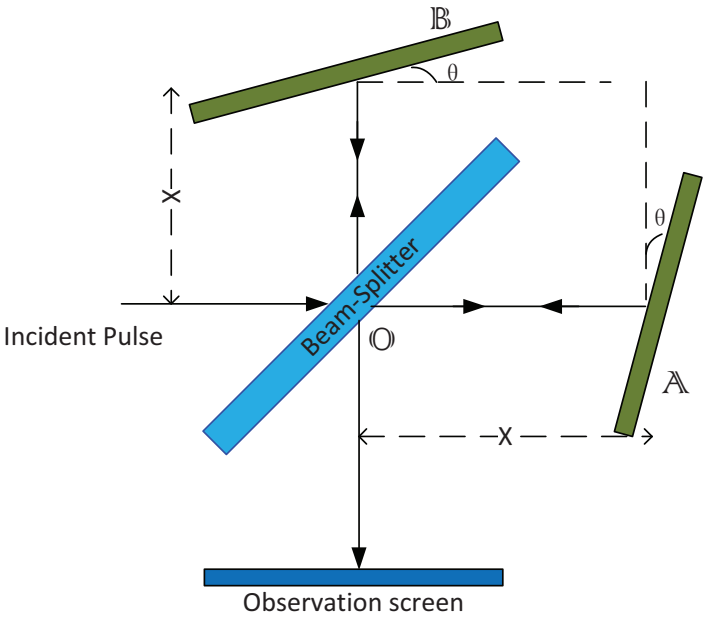

Figure 3.1: The setup of the Michelson interferometer.

Assuming a plane-wave pulse is incident on the interferometer, the observed field

is [46]

$$V(x;\omega) = \frac{1}{\sqrt{2}} V_0(\omega)[\exp(i\alpha\omega x) + \exp(-i\alpha\omega x)], \tag{3.4}$$

where $\alpha = \sin\theta/c$, and $V_0(\omega)$ is the frequency-domain representation of the incident pulse. The two-frequency cross-spectral density function associated with the pulse is defined as

$$W(x, \omega_1, \omega_2) = \langle V^*(x;\omega_1) V(x;\omega_2) \rangle \,, \tag{3.5}$$

where the brackets denote averaging over an ensemble of random pulses. Using the average and difference frequency coordinates $\omega = \frac{1}{2}(\omega_1 + \omega_2)$, $\Delta\omega = \omega_2 - \omega_1$ and the generalized Wiener-Khintchine theorem for non-stationary sources [47, 48, 49], the mutual coherence function in the observation plane is [46]

$$\Gamma(x;t,\Delta t) = \frac{1}{2}[\Gamma_0(t, \Delta t + 2\alpha x) + \Gamma_0(t, \Delta t + 2\alpha x) + \Gamma_0(t + \alpha x, \Delta t) + \Gamma_0(t - \alpha x, \Delta t)]. \tag{3.6}$$

Here $\Gamma_0(t, \Delta t) = \sqrt{I_0(t - \Delta t/2) I_0(t + \Delta t/2)}\gamma_0(t, \Delta t)$ is the mutual coherence function associated with the incident pulse train and $\gamma_0(t, \Delta t)$ is the complex degree of coherence of the incident field. Therefore, the intensity distribution reads [46]

$$\begin{aligned} I(x;t) = \frac{1}{2}[I_0(t + \alpha x) + I_0(t - \alpha x) + \sqrt{I_0(t - \alpha t) I_0(t + \alpha t)}\gamma_0(t, 2\alpha t) \\ + \sqrt{I_0(t - \alpha t) I_0(t + \alpha t/)}\gamma_0(t, -2\alpha t)]. \end{aligned} \tag{3.7}$$

Hence, the visibility, defined as [28]

$$v(x;t) = \frac{I_{max}(x,t) - I_{min}(x,t)}{I_{max}(x;t) + I_{min}(x;t)}, \tag{3.8}$$

can be shown to be given by the expression

$$V(x) = \frac{2\sqrt{I_0(t + \alpha x) I_0(t - \alpha x)}}{I_0(t + \alpha x) + I_0(t - \alpha x)} |\gamma_0(t, 2\alpha x)|. \tag{3.9}$$

Here, $\Delta t = 2\alpha x$ implies the time difference of the pulse which is related with the angle of two plane mirrors.

It is clear that Eq.(3.9) shows the visibility of fringes corresponding to the time difference of the pulse train. Hence, it is clear from Eq.(3.9) that if $I_0(t)$ is known, the complex degree of coherence γ_0 can be obtained from the measurement of the visibility. Furthermore, the mutual coherence function can be constructed from the measurement of the intensity of interference fringes which determines all the second-order coherence characteristics of the pulse train.

3.2 Complex Gaussian Representation of Statistical Pulses

In a coherent-mode decomposition of coherence theory, the mutual coherence function of the pulse can be expanded into a Mercer-type series as [14]

$$\Gamma(t_1, t_2) = \sum_n \lambda_n \phi_n^*(t_1)\phi_n(t_2), \tag{3.10}$$

where $\{\lambda_n\}$ are the eigenvalues and $\{\phi_n\}$ are the eigenfunctions of the integral equation

$$\int_{-\infty}^{\infty} \Gamma(t_1, t_2)\phi_n(t_1)dt_1 = \lambda_n \phi_n(t_2). \tag{3.11}$$

The modes of the pulse can be obtained by solving the integral equation Eq.(3.11). However, solving the integral equation is a formidable mathematical task. At the same time, analogous with the Glauber-Sudarshan $\mathcal{P}$-representation in quantum optics, the mutual coherence function of any partially coherent pulse can be expressed as an integral over an over-complete non-orthogonal set of complex Gaussian pulses [50].

We start by considering a time delayed by t_s Gaussian pulse with the carrier frequency shifted to ω_s. Its temporal profile is given by

$$\psi(t; t_s, \omega_s) = A \exp\left[-\frac{(t-t_s)^2}{2t_*^2}\right] e^{i\omega_s t}, \tag{3.12}$$

where A is a real amplitude and t_* is the width of the pulse. Using the dimensionless variables, $T = t/t_*$, $T_s = t_s/t_*$ and $\Omega_s = \omega_s t_*$, we obtain the following Gaussian profile

$$\psi_\alpha(T) = \frac{e^{-(Im\alpha)}}{\pi^{1/4}} \exp\left[-\frac{(T-\sqrt{2}\alpha)^2}{2}\right]. \tag{3.13}$$

Here a complex displacement α conveniently combines time delay and frequency shift viz

$$\alpha = \frac{1}{\sqrt{2}}(T_s + i\Omega_s). \tag{3.14}$$

We choose the amplitude A such that $\psi_\alpha(T)$ is normalized to unity,

$$\int_{-\infty}^{\infty} dT |\psi_\alpha(T)|^2 = 1. \tag{3.15}$$

It can be shown [50] that $\{\psi_\alpha(T)\}$ form an over-complete, complete but non-orthogonal, set such that

$$\int d^2\alpha \psi_\alpha^*(T_1)\psi_\alpha(T_2) = \delta(T_1 - T_2). \tag{3.16}$$

It was also shown in Ref [50] that the mutual coherence function of any partially coherent pulse, defined as

$$\Gamma(T_1, T_2) = \langle V^*(T_1)V(T_2)\rangle\,, \tag{3.17}$$

can be represented as

$$\Gamma(T_1, T_2) = \int d^2\alpha \mathcal{P}(\alpha)\psi^*_\alpha(T_1)\psi_\alpha(T_2), \tag{3.18}$$

where $\mathcal{P}(\alpha)$is a nonnegative function to guarantee non-negative definiteness of Γ. It is worth noticing that Eq(3.18) is reversible and inverting Eq. (3.18) we can obtain the classical $\mathcal{P}$ distribution function as [50]

$$\begin{aligned}\mathcal{P}(\alpha) = \frac{e^{|\alpha|^2}}{\pi^2}\int d^2\beta e^{|\beta|^2}\exp[\beta\times\alpha - \alpha\times\beta] \\ \times\int_{-\infty}^{\infty} dT_1\int_{-\infty}^{\infty} dT_2\Gamma(T_1, T_2)\psi^*_{-\beta}(T_1)\psi_\beta(T_2)\end{aligned} \tag{3.19}$$

Eq.(3.18) is a complex Gaussian representation of statistical pulses that can solve problems to find the appropriate complex Gaussian representation for any statistical pulse. It has been shown in [50] that the complex Gaussian pulses are not only mathematically well-behaved and physically realizable, but they also maintain their shapes on propagation in free space and linear media. In addition, the complex Gaussian representation can be employed to discover new partially coherent sources or represent the sources with given mutual coherence functions. In the following chapters, it is shown [51, 52] how one can generate novel partially coherent sources with nontrivial properties using the presented complex Gaussian representation of statistical pulses.

Chapter 4

Optical Coherence Gratings and Lattices

Liyuan Ma and Sergey A. Ponomarenko
Published in: Optics Letters, Vol. 39, Issue 23, pp. 6656-6659 (2014).
URL:http://www.opticsinfobase.org/ol/abstract.cfm?URI=ol-39-23-6656

There has lately been growing interest in designing novel partially coherent optical sources catering to a multitude of applications to optical communications, image transfer, and optical lithography, among others. Until recently, there have been known only a few classes of such sources, either spatial or temporal. Indeed, apart from seminal Gaussian Schell-model sources [32], only a few other classes emerged for which closed form analytical expressions for their cross-spectral densities or two-time correlation functions can be obtained. Twisted Gaussian Schell-model sources [53], which can be represented viz coherent mode decompositions of either Hermite-Gaussian [54] or Laguerre-Gaussian [55] modes, Bessel-correlated [20], modified-Bessel-correlated sources, generating partially coherent vortex fields [21], as well as dark and antidark diffraction-free sources [56] comprised all such known classes until late. All just mentioned partially coherent sources were either constructed or analyzed theoretically using the classic coherent mode representation of optical coherence theory [32]. Some such sources have also been experimentally realized to date [58, 59].

The introduction of a general representation for partially coherent sources, ensuring the generated fields to have bona fide correlation properties, has given new impetus to the field [60]. A multitude of partially coherent spatial and temporal sources were devised using the prescriptions of [60], including Gaussian sources with non-uniform correlations [61], flat-top field generating sources [62], Bessel-and Laguerre-Gaussian [63], circular cosine-Gaussian [64, 65], rectangular multi-Gaussian [66], temporal sources with tunable coherence profiles [67], and difference-Gaussian [69] Schell-model sources. In addition, new independent-elementary-source decomposition [70]

and complex Gaussian representation (CGR) [50] were introduced. While being particular forms of [60], the novel representations nonetheless open up alternative avenues for partially coherent source design. In particular, the CGR was shown to provide a convenient vehicle to devise trains of partially coherent pulses [50]. Moreover, due to over-completeness of the CGR modes, any partially coherent source has a CGR as was shown in [50]. Yet, the CGR power for new partially coherent source synthesis has barely been explored to date.

In this Letter, we employ the CGR to construct wide classes of temporal and spatial partially coherent sources which we term optical coherence gratings and lattices. All novel sources generate either statistically stationary pulses or statistically homogenous beams with Gaussian intensity profiles in the source plane. Thus, they are all of a Schell-model type. Yet, their coherence properties are periodic in time or space, and hence the name optical coherence gratings or lattices. In the temporal case, novel sources generate periodic trains of quasi-monochromatic components. In the spatial case, the novel sources give rise to periodic arrays of highly directional beams in the far zone of the source. The discovered sources can find applications to optical imaging with partially coherent light, optical information transfer through natural environments–where partially coherent pulses/beams are more robust in presence of media fluctuations–and to optical lithography, to name but a few.

Temporal coherence gratings.–According to the CGR, a two-time correlation function of any partially coherent source can be represented as [50]

$$\Gamma(T_1, T_2) = \int d^2\alpha \mathcal{P}(\alpha)\psi^*_\alpha(T_1)\psi_\alpha(T_2), \tag{4.1}$$

where $\alpha = \mathrm{Re}\,\alpha + i\mathrm{Im}\,\alpha$ is a complex variable; $d^2\alpha \equiv d(\mathrm{Re}\,\alpha)\,d(\mathrm{Im}\,\alpha)$, $\mathcal{P}(\alpha)$ is a nonnegative function to guarantee non-negative definiteness of Γ [32, 60, 50]. Hereafter, we will use dimensionless time and frequency variables, $T = t/\tau_\mathrm{p}$ and $\Omega = \omega\tau_\mathrm{p}$, where τ_p is a temporal width of the pulse, and assume any time variables to be scaled to τ_p. In the dimensionless variables, complex Gaussian modes,

$$\psi_\alpha(T) = \frac{e^{-(\mathrm{Im}\,\alpha)^2}}{\pi^{1/4}} \exp\left[-\frac{(T-\sqrt{2}\alpha)^2}{2}\right], \tag{4.2}$$

form an overcomplete, complete but non-orthogonal, set such that

$$\int d^2\alpha\, \psi^*_\alpha(T_1)\psi_\alpha(T_2) = \delta(T_1 - T_2). \tag{4.3}$$

As was discussed in detail elsewhere [50], the complex variable α incorporates time delays and frequency shifts of constituting Gaussian pulses.

Let us restrict ourselves to source classes for which the distribution function $\mathcal{P}$ has the form

$$\mathcal{P}(\alpha) = \sum_n \nu_n \delta(\alpha - \alpha_n), \quad \nu_n \geq 0. \tag{4.4}$$

It then follows from Eqs. (4.1) and (4.4) that

$$\Gamma(T_1, T_2) = \sum_n \nu_n \psi^*_{\alpha_n}(T_1)\psi_{\alpha_n}(T_2). \tag{4.5}$$

We note that Eq. (4.5) is in the form of pseudo-mode expansion discussed in [71] and ν_n characterizes energy distribution among the pseudo-modes.

A particularly interesting family of partially coherent Schell-model sources arises with the choice

$$\alpha_n = i\mathrm{Im}\,\alpha_n = i\frac{\pi n}{a\sqrt{2}}, \tag{4.6}$$

implying that there is no time delay, but consecutive Gaussian modes have equal relative frequency shifts. It follows from Eqs. (4.2), (5.6) and (4.6), after elementary algebra, that each such source has a Gaussian intensity,

$$I(T) \equiv \Gamma(T, T) = I_0 e^{-T^2}; \quad I_0 = \frac{1}{\sqrt{\pi}} \sum_n \nu_n, \tag{4.7}$$

and its temporal degree of coherence, defined as [32]

$$\gamma(T_1, T_2) \equiv \frac{\Gamma(T_1, T_2)}{\sqrt{I(T_1)I(T_2)}}, \tag{4.8}$$

can be expressed as

$$\gamma(T_1, T_2) = \frac{\sum_n \nu_n \exp\left[i\frac{\pi n}{a}(T_2 - T_1)\right]}{\sum_n \nu_n}. \tag{4.9}$$

We can infer from Eq. (4.9) that (i) discovered optical coherence gratings are statistically stationary and (ii) their coherence properties are time-periodic with a characteristic period of a (in scaled variables).

The energy spectrum, defined as [72]

$$S(\Omega) = \int_{-\infty}^{+\infty} dT_1 \int_{-\infty}^{+\infty} dT_2\, \Gamma(T_1, T_2) e^{i\Omega(T_1 - T_2)}, \tag{4.10}$$

reveals energy distribution among monochromatic components of the source. It follows from Eqs. (4.10), (4.8), and (4.9) after a straightforward algebra that up to an immaterial factor, energy spectra of novel sources are given by

$$S(\Omega) \propto \sum_n \nu_n e^{-(\Omega-\pi n/a)^2}. \tag{4.11}$$

It is a periodic Gaussian frequency comb with distinct quasi-monochromatic components which fail to overlap for a sufficiently small period a of the coherence grating.

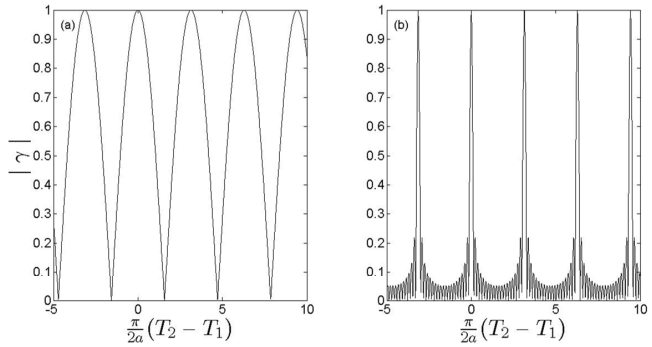

Figure 4.1: Modulus of the temporal degree of coherence given by Eq. (4.12) for (a) $N = 2$ and (b) $N = 20$.

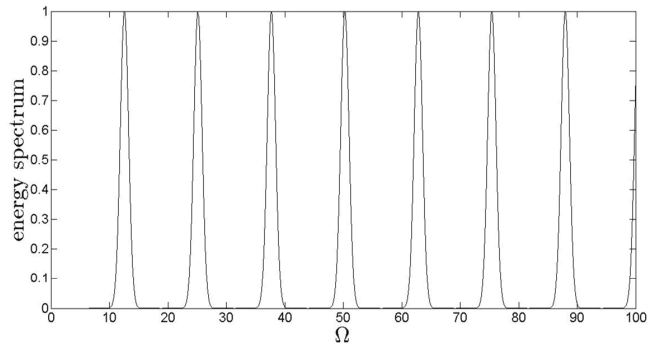

Figure 4.2: Energy spectrum in arbitrary units for the case of $N = 20$ equally weighted modes with the period $a = 0.25$.

Quantitative features of discovered coherence gratings and resulting statistical frequency combs depend on the mode energy distribution ν_n. Consider, for instance, a grating of finite number N of equally weighted complex Gaussians with $\nu_n = \nu = const$. Such a distribution yields a closed-from expression for γ such that

$$|\gamma(T_1, T_2)| = \left| \frac{\sin\left[\frac{\pi N}{2a}(T_2 - T_1)\right]}{N \sin\left[\frac{\pi}{2a}(T_2 - T_1)\right]} \right|, \tag{4.12}$$

which is displayed in Fig. 1 for two values of N. For large enough N, Eq. (4.12) is reminiscent of a classic pattern generated by illuminating a diffraction grating with a coherent plane wave in the far zone of the grating [30]. A quick glance at Fig.1b confirms the conclusion. The corresponding energy spectrum is exhibited in Fig. 2. It is clearly seen in the figure that the spectrum represents a periodic train of quasi-monochromatic components, provided the number of coherence grating lobes is sufficiently large, $N \gg 1$, and their period sufficiently small, $a < 1$.

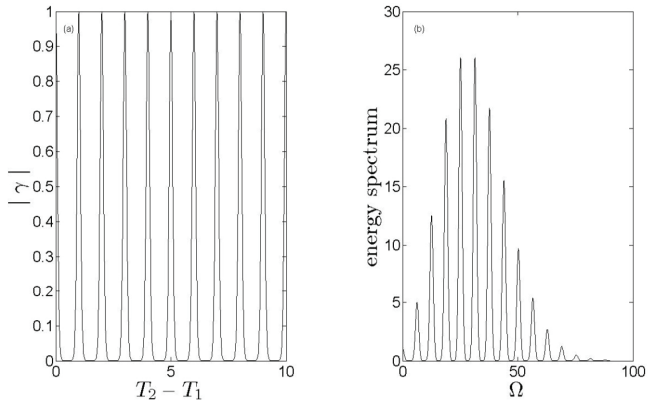

Figure 4.3: Magnitude of the temporal degree of coherence (a) and the energy spectrum in arbitrary units (b) for the case when the modes are distributed according to $\nu_n = \lambda^n/n!$ with $\lambda = 5$ and $a = 0.25$.

Another instructive example is furnished by an infinite number of CGs weighted according to $\nu_n = \lambda^n/n!$ where $\lambda > 0$ is a free parameter. The corresponding temporal degree of coherence sums to

$$|\gamma(T_1, T_2)| = \exp\left\{-2\lambda \sin^2\left[\frac{\pi(T_2 - T_1)}{2a}\right]\right\}. \tag{4.13}$$

We show the temporal degree of coherence and energy spectrum in Fig. 3. It is seen in the figure that this source possesses diffraction grating-like coherence properties resulting in a periodic energy spectrum as well. Unlike the case in Fig. 2, however, the spectral train is amplitude modulated here. Owning to qualitative agreement between the two cases, we can conclude that the whole class of sources, specified by (4.9), gives rise to optical coherence gratings.

Spatial coherence lattices.–A 2D generalization of the above describes spatial sources producing random beams. In the space-frequency representation, we seek the cross-spectral density of a beam field ensemble at a pair of points $\boldsymbol{\rho}_1$ and $\boldsymbol{\rho}_2$ in the source

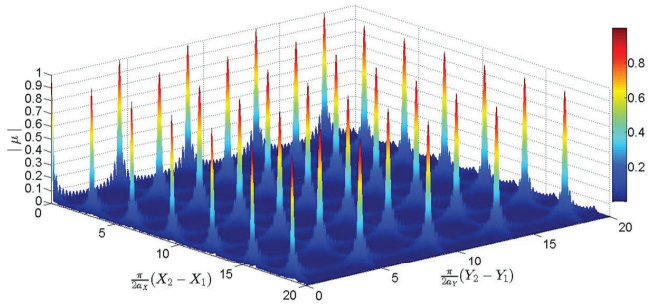

Figure 4.4: Magnitude of the spectral degree of coherence for a spatial coherence lattice composed of $N = 20$ equally weighted modes; the aspect ratio of lattice constants, $a_X/a_Y = 0.7$.

plane in a factorized form

$$W(\boldsymbol{\rho}_1, \boldsymbol{\rho}_2) = \prod_{s=X,Y} W(s_1, s_2). \tag{4.14}$$

Here $X = x/\sigma_{\mathrm{I}}$, $Y = y/\sigma_{\mathrm{I}}$ are dimensionless Cartesian coordinates scaled to an arbitrary spatial scale in the transverse pane of the beam; all spatial scales are assumed to be normalized to σ_{I} henceforth. As it will become clear in the following, σ_{I} does in this case coincide with the rms width of the source intensity profile. By analogy with the temporal case, each factor in the cross-spectral density product (5.1) can be expressed in terms of pseudo-modes as

$$W(s_1, s_2) = \sum_{n_s} \nu_{n_s} \psi^*_{\alpha_{n_s}}(s_1) \psi_{\alpha_{n_s}}(s_2), \tag{4.15}$$

where

$$\psi_{\alpha_{n_s}}(s) = \frac{e^{-(\mathrm{Im}\,\alpha_{n_s})^2}}{\pi^{1/4}} \exp\left[-\frac{(s - \sqrt{2}\alpha_{n_s})^2}{2}\right]. \tag{4.16}$$

It follows at once from the definition of the spectral degree of coherence [32, 73] that

$$\mu(\boldsymbol{\rho}_1, \boldsymbol{\rho}_2) \equiv \frac{W(\boldsymbol{\rho}_1, \boldsymbol{\rho}_2)}{\sqrt{I(\boldsymbol{\rho}_1) I(\boldsymbol{\rho}_2)}}. \tag{4.17}$$

Eqs. (4.15) and (4.16), (4.17), and a 2D analog of (4.6) yield a Gaussian source intensity profile,

$$I(\boldsymbol{\rho}) \equiv W(\boldsymbol{\rho}, \boldsymbol{\rho}) \propto e^{-(X^2+Y^2)}, \tag{4.18}$$

justifying the identification of the scaling length with the rms source width, and the

source coherence pattern in the form

$$\mu(\boldsymbol{\rho}_1, \boldsymbol{\rho}_2) = \prod_{s=X,Y} \frac{\sum_{n_s} \nu_{n_s} \exp\left[i\frac{\pi n_s}{a_s}(s_2 - s_1)\right]}{\sum_{n_s} \nu_{n_s}}. \tag{4.19}$$

In particular, the spectral degree of coherence magnitude of an optical lattice with $\nu_{n_s} = \nu = const$, $0 \leq n_s \leq N$, can be written explicitly as

$$|\mu(\boldsymbol{\rho}_1, \boldsymbol{\rho}_2)| = \frac{1}{N^2} \left| \prod_{s=X,Y} \frac{\sin\left[\frac{\pi N}{2a_s}(s_2 - s_1)\right]}{\sin\left[\frac{\pi}{2a_s}(s_2 - s_1)\right]} \right|. \tag{4.20}$$

To illustrate the spectral degree of coherence behavior, we display in Fig. 4, $|\mu|$ for a spatial coherence lattice composed of $N = 20$ equally weighted Gaussian beams with the lattice aspect ratio $a_X/a_Y = 0.7$. The lattice-like coherence behavior is transparent from the figure.

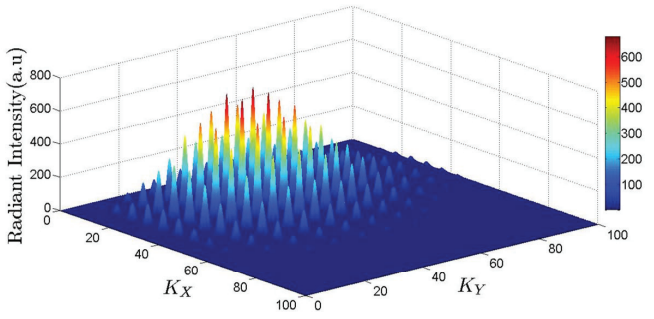

Figure 4.5: Radiant intensity distribution of a spatial coherence lattice composed of $N = 20$ modes distributed according to $\nu_{n_{X,Y}} = \lambda^{n_{X,Y}}/n_{X,Y}!$ with $\lambda = 5$ and $a = 0.25$; the aspect ratio of lattice constants, $a_X/a_Y = 0.7$.

The far-field angular distribution, generated by new sources, is specified by the radiant intensity J which can be expressed in the paraxial approximation as [32]

$$J(\mathbf{k}) = \int d\boldsymbol{\rho}_1 \int d\boldsymbol{\rho}_2 \, W(\boldsymbol{\rho}_1, \boldsymbol{\rho}_2) \exp[i\mathbf{k} \cdot (\boldsymbol{\rho}_1 - \boldsymbol{\rho}_2)], \tag{4.21}$$

where $\mathbf{k}$ is a 2D wave vector in the transverse plane of the source. Owning to a mathematical analogy between Eqs. (4.10) and (4.21), the radiant intensity distribution of a spatial coherence lattice can be expressed as

$$J(\mathbf{k}) \propto \prod_{s=X,Y} \sum_{n_s} \nu_{n_s} \, e^{-(K_s - \pi n_s/a_s)^2}, \tag{4.22}$$

where $K_{X,Y} = k_{x,y}\sigma_{\mathrm{I}}$. The radiant intensity is displayed in Fig. 5 in arbitrary units assuming the same weight distributions for the modes in the X and Y-directions, $\nu_{n_X} = \nu_{n_Y} = \lambda^{n_{X,Y}}/n_{X,Y}!$. For sufficiently small lattice constants $a_{X,Y}$ that we used, the angular distribution of the source radiation pattern is seen in the figure to be an amplitude modulated periodic lattice of highly directional individual lobes.

In summary, we introduced novel classes of partially coherent Schell-model spatial and temporal sources. New temporal sources, temporal coherence gratings, have Gaussian intensity profiles and periodic coherence properties, yielding periodic energy spectra in the form of frequency combs. New spatial sources, spatial coherence lattices, also have Gaussian intensity profiles and lattice-like spectral degrees of coherence. The latter circumstance causes them to generate lattice-like radiation patterns composed of highly directional individual lobes. Temporal coherence gratings and induced frequency combs can find metrology and optical communications applications. Spatial coherence lattices can be used for material processing, robust (speckle-free) imaging with partially coherent light and distortion-less information/image transfer through fluctuating natural environments such as the turbulent atmosphere.

Chapter 5

Free-Space Propagation of Optical Coherence Lattices and Periodicity Reciprocity

Liyuan Ma and Sergey A. Ponomarenko
Published in: Optics Express, Vol. 23, Issue 2, pp. 1848-1856 (2015)
URL:http://www.opticsinfobase.org/oe/abstract.cfm?URI=oe-23-2-1848

5.1 Abstract

We examine paraxial propagation of recently introduced optical coherence lattices in free space and demonstrate a novel phenomenon of periodicity reciprocity between their intensity and coherence properties. The periodicity reciprocity arises because an aperiodic source intensity profile of an optical coherence lattice evolves into a lattice-like far-field profile, while the periodic spectral degree of coherence at the source becomes aperiodic on free-space propagation. We discuss how the discovered periodicity reciprocity can make optical coherence lattices attractive for robust free-space optical communications.

5.2 Introduction

Owning to the immunity of partially coherent beams to speckle formation in optical imaging and their robustness to natural media fluctuations, research into optical communications with partially coherent light has recently enjoyed a renaissance. In particular, the potential of propagation-invariant (diffraction-free) coherent and partially coherent beams and pulsed beams for distortion-less free-space information/image transfer applications has been recognized [74, 75]. Moreover, special classes of diffraction-free partially coherent beams, such as dark diffraction-free beams [56], can serve as versatile optical traps for neutral nano-particles or even

atoms. Shape-invariant (self-similar) partially coherent beams can also be useful in free-space speckle-free image transfer and free-space optical communications. Several prominent classes of self-similar partially coherent beams have been discovered to date, including Gaussian Schell-model [60, 76], and twisted Gaussian Schell-model [18, 55, 58] beams. By the same token, partially coherent modified-Bessel vortex beams [21], separable vortex beams [59] as well as some others [71] are shape invariant because they admit a coherent-mode decomposition [32] in terms of self-similar Laguerre-Gaussian [21, 59] or Hermite-Gaussian [71] modes.

Although non-shape-invariant partially coherent beams are fairly useless for optical communication applications, they can possess desirable attributes for far-field coherence or radiation pattern generation on demand. For instance, while J_0-correlated partially coherent beams have drastically evolving coherence properties on free-space propagation [20, 77], various families of multi-Gaussian Schell-model beams can either form a flat-top radiation pattern [62] or split on propagation [63]. On the other hand, non-uniformly correlated Gaussian beams can have their peak intensity positions shift upon free-space propagation [61]. Some non-shape-invariant partially coherent beams were shown to form stable structures on short-distance propagation through the turbulent atmosphere [23, 78, 64].

Partially coherent beams with periodic cross-spectral densities present yet another important class. The significance of such beams for imaging is revealed by the existence of Lau [69, 79] and Talbot [79, 80, 81, 82, 83, 84] self-imaging effects for partially coherent light. In the first instance, self-imaging arises on paraxial propagation of light generated by completely incoherent sources with periodic intensity profiles. In the second instance, though, the periodicity of scalar cross-spectral densities [79, 80, 82, 83] or cross-spectral density tensors [84] for polarized or partially polarized sources, respectively, is required for self-imaging. Lately, a new class of partially coherent beams, optical coherence lattices (OCL), was introduced [51] using recently developed complex Gaussian representation (CGR) of statistical pulses and beams [50]. The newly discovered OCLs have aperiodic (Gaussian) intensity profiles and statistically homogeneous, periodic coherence properties, precluding Talbot self-imaging in free space. The natural question then arises: Can OCLs be useful for optical imaging, communications, or information transfer?

To address this issue, we examine free-space evolution properties of OCLs in this work. In particular, we explore how the intensity profile and spectral degree of coherence of an OCL change on paraxial propagation. We discover periodicity reciprocity between the intensity and coherence properties of optical coherence lattices. The new phenomenon manifests itself when an aperiodic, Gaussian intensity profile of the source evolves into a periodic array of lobes in the far zone, whereas the initially periodic spectral degree of coherence loses its periodicity on lattice propagation. Thus, the spectral degree of coherence periodicity at the source is transferred to the far-field intensity profile periodicity. We suggest that the phenomenon can find applications to robust free-space optical communications.

5.3 Problem formulation and preliminary analysis

We begin by recalling that the cross-spectral density of a beam field ensemble of recently discovered [51] optical coherence lattices at a pair of points (X_1, Y_1) and (X_2, Y_2) in the source plane can be expressed in a factorized form as

$$W(X_1, Y_1, X_2, Y_2, 0) = \prod_{s=X,Y} W(s_1, s_2, 0). \tag{5.1}$$

Here $X = x/\sigma_{\rm I}$, $Y = y/\sigma_{\rm I}$ are dimensionless Cartesian coordinates scaled to the rms width $\sigma_{\rm I}$ of the source intensity profile and we will drop an irrelevant dependence of the cross-spectral density on frequency henceforth. Using the CGR of statistical beams [50], each factor $W(s_1, s_2, 0)$ can be expressed as

$$W(s_1, s_2, 0) = \int d^2\alpha\, \mathcal{P}_s(\alpha)\psi^*_\alpha(s_1, 0)\psi_\alpha(s_2, 0), \tag{5.2}$$

where $\mathcal{P}_s$ is a nonnegative distribution function to guarantee non-negative definiteness of W and $d^2\alpha \equiv d\,(\mathrm{Re}\,\alpha\,)\,d\,(\mathrm{Im}\,\alpha)$. The pseudo-modes $\{\psi_\alpha(s, 0)\}$ are normalized,

$$\int ds\, \psi^*_\alpha(s, 0)\psi_\alpha(s, 0) = 1, \tag{5.3}$$

and form an over-complete set such that

$$\int d^2\alpha\, \psi^*_\alpha(s_1, 0)\psi_\alpha(s_2, 0) = \delta(s_1 - s_2). \tag{5.4}$$

In the OCL case [51], $\mathcal{P}_s$ has the form

$$\mathcal{P}_s(\alpha) = \sum_{n_s} \nu_{n_s}\delta(\alpha - \alpha_{n_s}), \quad \nu_{n_s} \geq 0. \tag{5.5}$$

On substituting from Eq. (5.5) into (5.2), we arrive at a pseudo-mode expansion of $W(s_1, s_2, 0)$ in the form

$$W(s_1, s_2; 0) = \sum_{n_s} \nu_{n_s} \psi^*_{\alpha_{n_s}}(s_1, 0) \psi_{\alpha_{n_s}}(s_2, 0). \tag{5.6}$$

Here the mode weight distributions ν_{n_s} specify the intensity associated with each mode and

$$\alpha_{n_s} = \frac{i\pi n_s}{a_s\sqrt{2}}, \tag{5.7}$$

where a_s is a (dimensionless) lattice constant in the s-direction and n_s is an integer. Each lattice pseudo-mode at the source can be expressed as

$$\psi_{\alpha_{n_s}}(s, 0) = \frac{e^{-(\mathrm{Im}\,\alpha_{n_s})^2}}{\pi^{1/4}} \exp\left[-\frac{(s - \sqrt{2}\alpha_{n_s})^2}{2}\right]. \tag{5.8}$$

Next, let us recall that the cross-spectral density function of any partially coherent beam ensemble, propagating in free space, obeys the paraxial Wolf equation [32] which we re-write in the dimensionless form as

$$(2i\partial_Z + \nabla^2_{\perp 2} - \nabla^2_{\perp 1}) W(X_1, Y_1, X_2, Y_2; Z) = 0. \tag{5.9}$$

The dimensionless propagation distance Z is naturally measured in Rayleigh range units z_{R} corresponding to a fully coherent source of the width σ_{I}, $z_{\mathrm{R}} = k\sigma^2_{\mathrm{I}}$. Owning to the separability of Eq. (5.9) in the Cartesian coordinates, we can factorize W in any transverse plane $Z = const > 0$, i. e.,

$$W(X_1, Y_1, X_2, Y_2; Z) = \prod_{s=X,Y} W(s_1, s_2; Z), \tag{5.10}$$

where each factor can be expanded into the pseudo-modes as

$$W(s_1, s_2; Z) = \sum_{n_s} \nu_{n_s}\, \psi^*_{\alpha_{n_s}}(s_1, Z) \psi_{\alpha_{n_s}}(s_2, Z). \tag{5.11}$$

On substituting from Eqs. (5.10) and (5.11) and separating spatial variables in the transverse plane, we obtain a paraxial wave equation for each pseudo-mode as

$$(2i\partial_Z + \partial^2_s) \psi_{\alpha_{n_s}}(s, Z) = 0. \tag{5.12}$$

The appropriate solution to Eq.(5.12), subject to the initial condition at the source (5.8), can be obtained in the form

$$\psi_{\alpha_{n_s}}(s,Z)=\frac{e^{-(\mathrm{Im}\,\alpha_{n_s})^2}}{\pi^{1/4}(1+iZ)^{1/2}}\exp\left[-\frac{(s-\sqrt{2}\alpha_{n_s})^2}{2(1+iZ)}\right]. \tag{5.13}$$

It follows from Eqs. (5.11) and (5.13), after elementary algebra, that the cross-spectral density of an optical lattice in any transverse plane $Z=const$ is given by Eq. (5.10) with

$$W(s_1,s_2;Z)=\frac{\exp\left[\frac{i(s_2^2-s_1^2)}{2R(Z)}\right]}{\sqrt{\pi(1+Z^2)}}\sum_{n_s}\nu_{n_s}\exp\left\{\frac{i\pi n_s}{a_s}\left[\frac{s_2-s_1}{\sigma^2(Z)}\right]\right\}$$
$$\times\exp\left[-\frac{(s_1-\pi n_s Z/a_s)^2+(s_2-\pi n_s Z/a_s)^2}{2\sigma^2(Z)}\right]. \tag{5.14}$$

In Eq. (5.14), $R(Z)$ and $\sigma(Z)$ are dimensionless radius of the curvature and rms width of the beam specified by the expressions

$$R(Z)=Z+1/Z,\qquad \sigma(Z)=\sqrt{1+Z^2}. \tag{5.15}$$

In particular, the intensity profile of an OCL field can be found as

$$I(X,Y;Z)\equiv\prod_{s=X,Y}W(s,s;Z)=\frac{1}{\pi(1+Z^2)}\prod_{s=X,Y}\sum_{n_s}\nu_{n_s}\exp\left[-\frac{(s-\pi n_s Z/a_s)^2}{\sigma^2(Z)}\right]. \tag{5.16}$$

A qualitative analysis of Eq. (5.16) indicates that an initially Gaussian beam starts branching out into a Gaussian lattice with the individual Gaussian node intensities decreasing in amplitude on propagation. Further, each Gaussian spreads and the distance between the adjacent lattice nodes increases. Over several Rayleigh distances, the rates of node width spreading and adjacent node separation are both proportional to Z. However, the latter exceeds the former, provided the lattice constant is small enough, $a_{X,Y}\leq\pi$. Under the circumstances, the structural stability of the lattice is no longer compromised. Otherwise, individual lattice nodes can start overlapping over a certain propagation distance, resulting in annihilation of the overall beam lattice structure. Hereafter, we will restrict our analysis to OCLs maintaining their lattice structure in the far-zone due to their potential for free-space optical communications.

The spectral degree of coherence behavior follows from its definition [32, 68, 85]

$$\mu(X_1,Y_1,X_2,Y_2;Z)=\frac{W(X_1,Y_1,X_2,Y_2;Z)}{\sqrt{I(X_1,Y_1;Z)}\sqrt{I(X_2,Y_2;Z)}}, \tag{5.17}$$

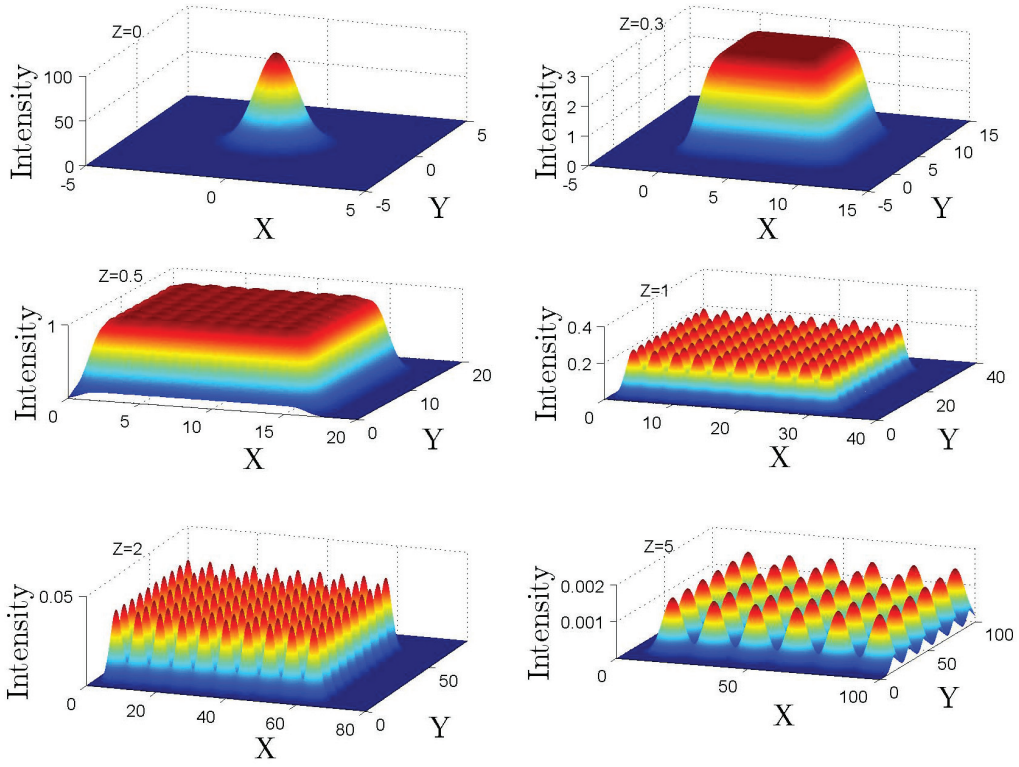

Figure 5.1: Intensity profile (in arbitrary units) of a uniformly distributed OCL for several propagation distances Z. The lattice is composed of $N = 10$ lobes and the lattice constant is $a = 1$.

together with Eqs. (5.10), (5.14) and (5.16). According to the van Cittert-Zernike theorem of the optical coherence theory [28], the lattices must become progressively more coherent on free-space propagation. In the following section, we illustrate the evolution of lattice intensity and spectral degree of coherence for several nontrivial cases.

5.4 The OCL intensity and spectral degree of coherence propagation in free space

We first consider an OCL composed of a finite number N of uniformly distributed complex Gaussian pseudo-modes such that

$$\nu_{n_X} = \nu_{n_Y} = \nu_0 = const; \qquad 0 \leq n_{X,Y} \leq N. \tag{5.18}$$

Under these conditions, the lattice intensity profile and spectral degree of coherence

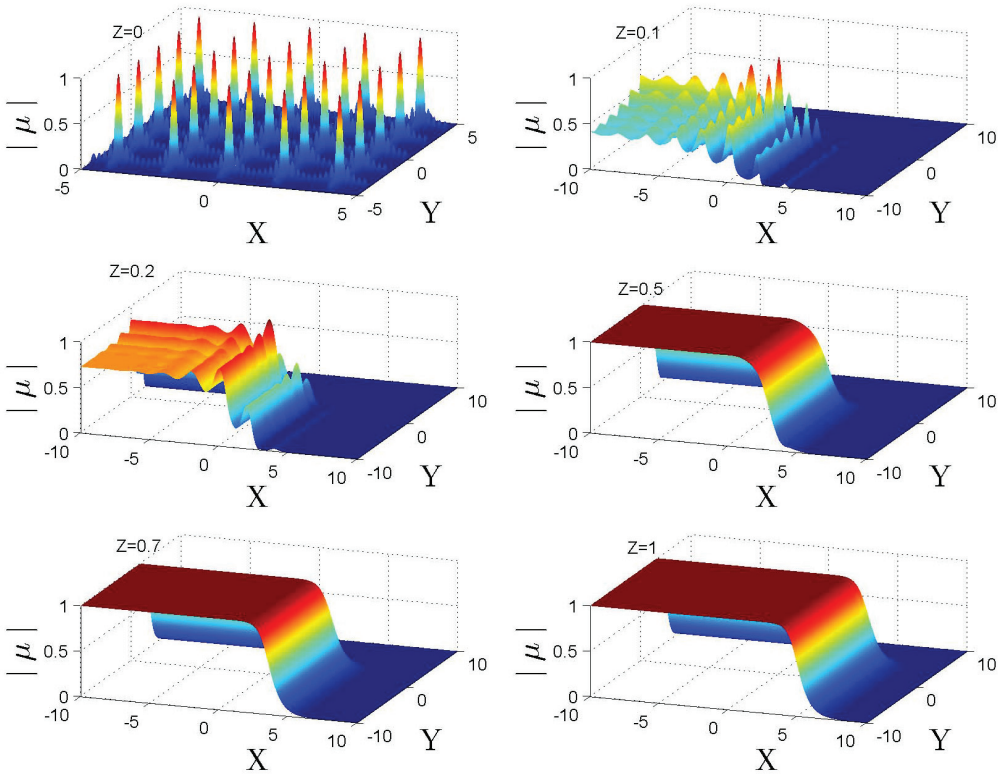

Figure 5.2: Magnitude of the spectral degree of coherence of a uniformly distributed OCL for several propagation distances Z. The lattice is composed of $N = 10$ lobes and the lattice constant is $a = 1$.

at the source can be evaluated in closed forms as [51]

$$I(X, Y, 0) \propto e^{-(X^2+Y^2)}, \tag{5.19}$$

up to an immaterial constant, and

$$|\mu(X_1, Y_1, X_2, Y_2; 0)| = \left| \frac{\sin\left[\frac{\pi N}{2a}(X_2 - X_1)\right] \sin\left[\frac{\pi N}{2a}(Y_2 - Y_1)\right]}{N^2 \sin\left[\frac{\pi}{2a}(X_2 - X_1)\right] \sin\left[\frac{\pi}{2a}(Y_2 - Y_1)\right]} \right|, \tag{5.20}$$

respectively. In deriving Eq. (5.20) we assumed, for simplicity, that the lattice constants in the X- and Y-directions are the same, $a_X = a_Y = a$.

Let us now display the behavior of the intensity and magnitude of the spectral degree of coherence of the lattice on its evolution with Z according to Eqs. (5.14) through (5.17). The intensity evolution is exhibited in Fig. 1, while the modulus of the spectral degree of coherence is shown in Fig. 2.

As can be inferred from Fig.1, an originally aperiodic in intensity Gaussian beam forms a lattice on propagation. In accord with the above qualitative analysis after

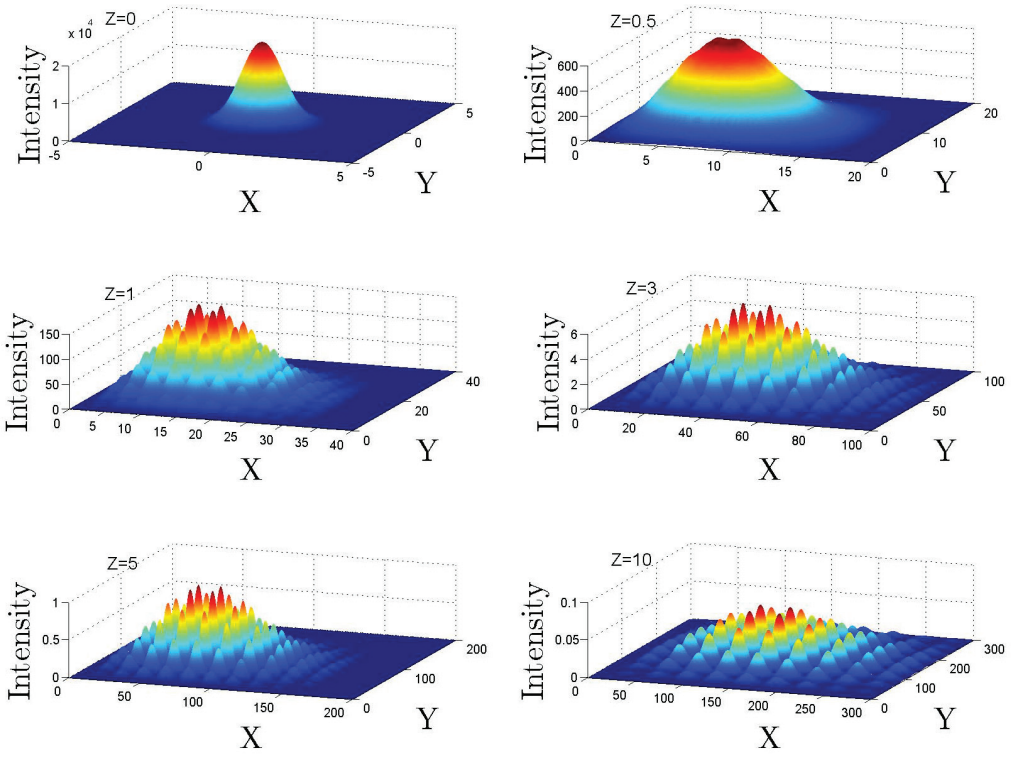

Figure 5.3: Intensity profile (in arbitrary units) of a symmetric, non-uniformly distributed OCL for several propagation distances Z. The the lattice constant is $a = 1$ and the weight distribution parameter is $\lambda = 5$.

the intensity lattice has been formed, the lattice structure of the OCL remains intact, provided the lattice constant is not too large. The subsequent propagation into the far zone causes the lattice to expand and the individual node intensity maxima to decrease. The more-or-less stable lattice structure is formed over the Rayleigh range.

A quick look at Fig. 2 prompts the conclusion that the lattice structure of the source degree of coherence is destroyed on propagation, yielding an aperiodic spectral degree of coherence with the portion of the beam having $|\mu| = 1$ gradually increasing on propagation. Thus, the OCLs become progressively more coherent in agreement with the van Cittert-Zernike theorem. More instructively, however, we observe a curious reciprocity between the periodicity of OCL intensity and spectral degree of coherence. Indeed, while each lattice source has an aperiodic (Gaussian) intensity profile and a periodic spectral degree of coherence, a periodic intensity profile and aperiodic spectral degree of coherence emerge in the far zone of the source. We can conclude that, at least for uniformly distributed OCLs, the periodicity is transferred

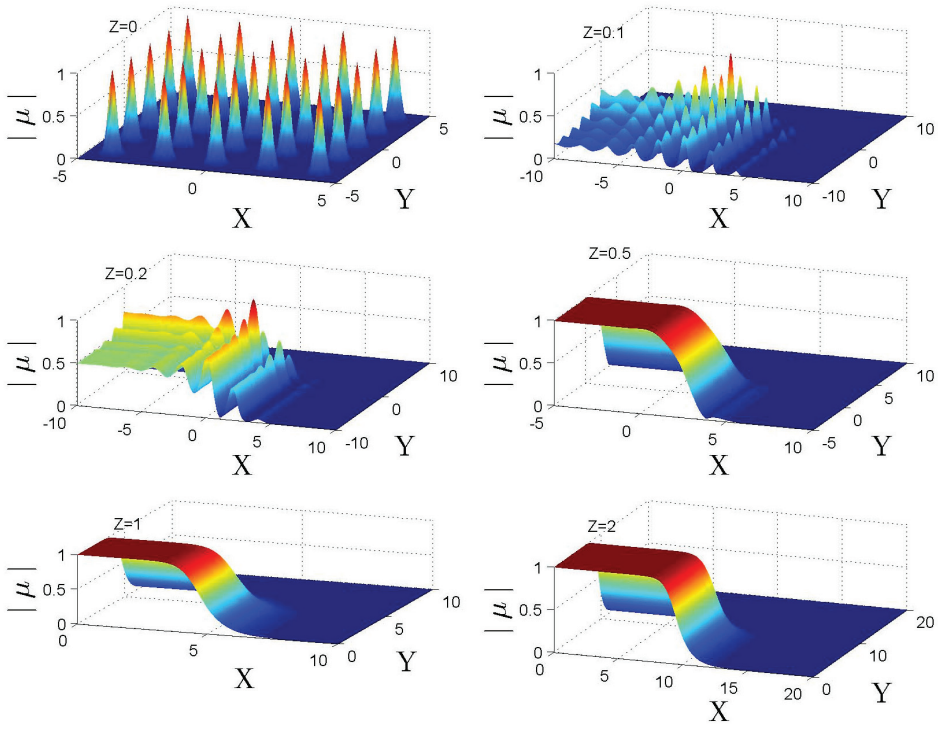

Figure 5.4: Magnitude of the spectral degree of coherence of a symmetric, non-uniformly distributed OCL for several propagation distances Z. The lattice constant is $a = 1$ and the weight distribution parameter is $\lambda = 5$.

from the degree of coherence at the source to the far-field intensity.

To determine whether the discovered periodicity reciprocity is generic to OCLs, we will examine non-uniformly distributed OCL propagation. To this end, we consider an OCL with a nonuniform distribution of pseudo-modes as

$$\nu_{n_s} = \mathcal{A}\frac{\lambda_s^{n_s}}{n_s!}; \qquad n_s \geq 0, \tag{5.21}$$

where $\mathcal{A}$ is a positive constant. The corresponding source intensity is again Gaussian and the spectral degree of coherence at the source can be inferred from the Eqs. (5.14) through (5.17) as well as (5.21) such that

$$|\mu(X_1, Y_1, X_2, Y_2; 0)| = \exp\left\{-2\sum_{s=X,Y}\lambda_s \sin^2\left[\frac{\pi(s_2 - s_1)}{2a_s}\right]\right\}. \tag{5.22}$$

We can then display the nonuniform OCL intensity and spectral degree of coherence behavior in Figs. 3 and 4. We assume, for simplicity, that the lattices are symmetric with $a_X = a_Y = a$ and identically distributed along the X- and Y-axes such that $\lambda_X = \lambda_Y = \lambda$.

Figures 3 and 4 reveal the same key trends as do Figs. 1 and 2. Namely, the initially aperiodic source intensity profile gives rise to a periodic lattice and the initially periodic source spectral degree of coherence evolves into an aperiodic one. Thus, periodicity reciprocity is confirmed for non-uniformly distributed lattices as well and hence it appears to be a generic property of discovered OCLs. The only qualitative difference in the evolution of nonuniform from uniform OCLs, which is manifest on comparing Figs. 1 and 3, appears to be the intensity profile modulation of the former caused by a nonuniform distribution of their pseudo-modes.

5.5 Conclusions

In this work, we have explored the intensity and spectral degree of coherence evolution of recently introduced optical coherence lattices. We have shown that while an aperiodic source intensity profile of an OCL–which always happens to be Gaussian–develops spatial periodicity on paraxial propagation in free space, the initially lattice-like spectral degree of coherence loses its spatial periodicity on OCL propagation. Thus, the OCL periodicity has a reciprocity property: coherence-periodic OCLs at the source give rise to intensity-periodic far-field patterns. The discovered OCL periodicity reciprocity is shown to be generic for OCLs and it can be utilized in robust free-space optical communications. Indeed, specific information, encoded in an OCL via the periodicity of its spectral degree of coherence at the source, can be transmitted through a free-space link. The periodicity reciprocity of OCLs ensures that the encoded information is contained in the OCL far-field intensity pattern. The information can then be decoded by simply interrogating the OCL far-field intensity profile at the receiver.

Chapter 6

Conclusion

In this thesis, we introduce a new class of partially coherent temporal and spatial sources, optical coherence gratings/lattices. We also examine the propagation properties of the new partially coherence sources in free space.

In the first paper, using the complex Gaussian representation, we construct a new class of partially coherent sources in temporal and spatial domains. Novel sources generate either pulses with statistically stationary or beams with statistically homogeneous coherence properties in the source plane. Further, the novel sources also show periodic coherence properties. In particular, the new temporal sources, the so-called optical coherence gratings, show diffraction grating-like coherence properties corresponding to a periodic energy spectrum in the source plane. Meanwhile, the new spatial sources, spatial coherence lattices, have a lattices-like spectral degrees of coherence which cause them to generate lattice-like radiation patterns. We also proved that spatial coherence lattices can produce periodic lattices of highly directional beams in the far zone.

In the second paper, we studied propagation properties of the newly discovered spatial coherence lattices. We explored the intensity and the spectral degree of coherence of optical coherence lattices in several nontrivial cases and discovered an interesting novel phenomenon, the periodicity reciprocity. In particular, an initially Gaussian beam branches out into a Gaussian lattice with individual Gaussian mode intensities decreasing in amplitude on free-space propagation. At the same time, the periodicity of the complex degree of coherence of the source is destroyed during propagation as the optical coherence lattices gradually become more coherent on propagation. Thus, the periodicity can be transfered from the degree of coherence at the source to the far-field intensity. In the thesis, we illustrate the evolution of the intensity and complex degree of coherence in several cases and find that the periodicity reciprocity occurs in each case.

We expect the periodicity reciprocity to make these new sources useful in robust free-space optical communications. In the future, we hope to find more applications to material processing, robust imaging with partially coherent light and distortion-less information/image transfer through fluctuating media such as the turbulent atmosphere.

Bibliography

[1] T. H. Maiman, "Stimulated optical radiation in ruby," Nature (London) **187**, 493–494.

[2] Townes and C. Hard, "The first laser," University of Chicago Retrieved May 15, 2008.

[3] J. P. Gaska, C. Tai, and G. A. Geri, "Laser-speckle properties and their effect on target detection," J. Soc. Inf. Displ. **15**, 1023–1028 (2007).

[4] J. M. Artigas, A. Felipe, and M. J. Buades, "Contrast sensitivity of the visual system in speckle imagery," J. Opt. Soc. Am. A **11**, 2345–2349 (1994).

[5] M. S. Belenkii, A. I. Kon, and V. L. Mironov, "Turbulent distortions of the spatial coherence of a laser beam," Sov. J. Quantum Electron. **7**, 287–290 (1977).

[6] R. L. Fante, "The effect of source temporal coherence on light scintillations in weak turbulence," J. Opt. Soc. Am. **69**, 71–73 (1979).

[7] E. Wolf, "Coherence and radiometry," J. Opt. Soc. Am. **68**, 6–17 (1978).

[8] E. Wolf, "New theory of partial coherence in the space-frequency domain. Part II:Steady-state fields and higher-order correlations," J. Opt. Soc. Am. A **3**, 76 (1983).

[9] E. Wolf and E. Collett, "Partially coherent sources which produce the same far-field intensity distribution as a laser," Opt. Commun. **25**, 293-296 (1978).

[10] B. E. A. Saleh, "Intensity distribution due to a partially coherent field and the Collett-Wolf equivalence theorem in the Fresnel zone," Opt. Commun. **30**, 135 (1979).

[11] S. A. Ponomarenko and E. Wolf, "Universal structure of field correlations within a fluctuating medium", Phys. Rev. E, **65**, 016602 (2001).

[12] S. A. Ponomarenko, J-J. Greffet, and E. Wolf, "The diffusion of partially coherent beams in turbulent media", Opt. Commun. **128**, 1 (2002).

[13] E. Wolf, "New spectral representation of random source and of the partially coherent fields that they generate," Opt. Commun. **38**, 3–6 (1981).

[14] E. Wolf, "New theory of partial coherence in the space-frequency domain. Part 1: Spectra and cross-spectra of steady-state source," J. Opt. Soc. Am. **72**, 343–351 (1982).

[15] L. Mandel and E. Wolf, "Complete coherence in the space-frequency domain," Opt. Commun. **36**, 247–249 (1981).

[16] P. De Santis, F. Gobi, G. Guattari and C. Palma, "An example of a Collett-Wolf source," Opt. Commun. **29**, 256 (1979).

[17] D. J. Farina, L. M. Narducca and E. Collett, "Generation of highly directional beams from a globally incoherent source," Opt. Commun. **32**, 203 (1980).

[18] R. Simon and N. Mukunda, "Twisted Gaussian Schell-model beams," J. Opt. Soc. Am. A **10**, 95–109 (1993).

[19] K. Sundar, N. Mukunda, and R. Simon, "Twisted Gaussian Schell-model beams. II. Spectrum analysis and propagation characteristics," J. Opt. Soc. Am. A **10**, 2017–2023 (1993).

[20] F. Gori, G. Guattari, and C. Padovani, "Modal expansion for J_0-correlated Schell-model sources," Opt. Commun. **64**, 311–316 (1987).

[21] S. A. Ponomarenko, "A class of partially coherent beams carrying optical vortices," J. Opt. Soc. Am. A **18**, 150–156 (2001).

[22] J. C. Ricklin, F. M. Davidson and T. Weyrauch, "Free-space laser communication using a partially coherent laser source," Proc. SPIE **4538**, 13 (2002).

[23] H. T. Eyyuboglu and Y. Baykal, "Transmittance pf partially coherent cosh-Gaussian, cos-Gaussian, and annular beams through turbulence," Opt. Commun., **278** 17–22 (2007).

[24] D. F. V. James, E. Wolf, "Some new aspects of Young's interference experiment," Phys. Lett. A **157**, 6 (1991).

[25] H. C. Kandpal, J. S. Vaishya, M. Chander. K. Sacena, D. S. Metha and K. C. Joshi, "Spectral changes due to source correlation in Young's interference experiment," Phys. Lett. A **167**, 114, (1992).

[26] D. S. Metha, K.C. Joshi, "Field correlations from spectral measurements in Young's interference experiment," Phys. Lett. A **167**, 120–122 (1992).

[27] M. Sansarsiero, F. Cori, "Spectral changes in a Young interference pattern," Phys. Lett. A **167**, 123 (1992).

[28] E. Wolf, *Introduction to the Theory of Coherence and Polarization of Light* (Cambridge Univ. Press, Cambridge, UK, 2007).

[29] M. Born, and E. Wolf, *principles of optics*, (Cambridge University Press, Cambridge, 1999).

[30] J. W. Goodman, *Introduction to Fourier Optics,* (McGraw Hill, New York, 1998) 2nd edition.

[31] N. Wiener, "Generalized harmonic analysis," Acta Math. **55**, 177-258 (1930).

[32] L. Mandel and E. Wolf, *Optical Coherence and Quantum Optics,* (Cambridge University Press, Cambridge, 1997).

[33] F. Smithies, *Integral Equations,* (Cambridge University Press, Cambridge,1970).

[34] F. Riecz And B. Sz. Nagy, *Functional Analysis,* (Ungar, New York, 1955).

[35] L. Mandel and E. Wolf, "Spectral coherence and the concept of cross-spectral purity," J. Opt. Soc. Am. A **66**, 529-535 (1976).

[36] Ari T. Friberg, Ronald J. Sudol, "The spatial coherence properties of Gaussian Schell-model beams," J. Mod. Opt. **30**, 1075–1097(1983).

[37] H. Kogelnik, and T. Li, "Laser beam resonators, Proc. IEEE **54**, 1312-1329 (1966).

[38] Ari T. Friberg and Ronald J Sudol, "Propagation parameters of Gaussian Schell-model beams," Opt. Commun. **41**, 383–387 (1982).

[39] P. Paakkonen, J. Turunen, P. Vahimaa, A. T. Friberg, and F. Wyrowski, "Partially coherent Gaussian pulses, Opt. Commun. **204**, 53-58 (2002).

[40] M. Bertolotti, A. Ferrari and L Sereda, "Coherence properties of nonstationary polychromatic light sources," J. Opt. Soc. Am. B **12**, 341–347 (1995).

[41] H Lajunen, J Tervo and P Vahimaa, "Theory of spatially and spectrally partially coherent pulses," J. Opt. Soc. Am. A **22**, 1536-1545 (2005).

[42] A. Forbes, *"Laser beam propagation: Generation and Propagation of Customized Light, Chapter 10"* (CRC Press, NW) (2014)

[43] E. Wolf, G. S. Agarwal, "Coherence theory of laser resonator modes," J. Opt. Soc. Am. A **1**, 541 (1984).

[44] A. Michelson,E, Morley, "On the Relative Motion of the Earth and the Luminiferous Ether," American Journal of Science **34**, 333-345 (1881).

[45] R. Dutta, J. Turunen, and Ari. T. Friberg, "Michelson's interferometer and the temporal coherence of pulse trains," Opt. Lett. **40**, 166–169 (2015).

[46] M. Bertolotti, L. Sereda, and A. Ferrari, "Application of the spectral representation of stochastic processes to the study of non-stationary light radiation: a tutorial," Pure Appl. Opt.**6**, 153-171 (1997).

[47] L.Sereda, M. Bertolotti and A. Ferrari, "Coherence properties of nonstationary light wave fields," J. Opt. Soc. Am. A **15**, 695–705 (1998).

[48] C.H. Page, "Instantaneous Power Spectra," Appl. Phys. **23**, 103 (1952).

[49] D.G. Lampard, "Generalization of the WienerKhintchine Theorem to Nonstationary Processes," Appl. Phys. **25**, 803 (1954).

[50] S. A. Ponomarenko, "Complex Gaussian representation of statistical pulses," Opt. Express **19**, 17086 (2011).

[51] L. Ma and S. A. Ponomarenko, "Optical coherence gratings and lattices," Opt. Lett. **39**, 6656-6659 (2014)

[52] L. Ma, and S. A. Ponomarenko, "Free-space Propagation of optical coherence lattices and periodicity reciprocity," œ**23**, 1848-1856 (2015)

[53] R. Simon and N. Mukunda, "Twisted Gaussian Schell-model beams," J. Opt. Soc. Am. A **10**, 95–109 (1993).

[54] R. Simon, and N. Mukunda, "Twisted Gaussian Schell-model beams I: Symmetry structure and normal mode sopectrum," J. Opt. Soc. Am. A **10**, 2008–2016 (1993).

[55] S. A. Ponomarenko, "Twisted Gaussian Schell-model solitons," Phys. Rev. E **64**, 036618 (2001).

[56] S. A. Ponomarenko, W. Huang, and M. Cada, "Dark and antidark diffraction-free beams," Opt. Lett. **32**, 2508–2510 (2007).

[57] L. Ma, and S. A. Ponomarenko, "Free-space Propagation of optical coherence lattices adn periodicity reciprocity," œ**23**, 1848–1856 (2015).

[58] A. T. Friberg, E. Tervonen, and J. Turunen, "Interpretation and experimental demonstration of twisted Gaussian Schell-model beams," J. Opt. Soc. Am. A **11**, 1818–1826 (1994).

[59] G. V. Bogatyryova, C. V. Fel'de, P. V. Polyanskii, S. A. Ponomarenko, M. S. Soskin, and E. Wolf, "Partially coherent separable vortex beams," Opt. Lett. **28**, 878–880 (2003).

[60] F. Gori and M. Santarsiero, "Devising genuine spatial correlation functions," Opt. Lett. **32**, 3531–3533 (2007).

[61] H. Lajunen and T. Saastamoinen, "Propagation characteristics of partially coherent beams with spatially varying correlations," Opt. Lett. **36**, 4104–4106 (2011).

[62] S. Sahin and O. Korotkova, "Light sources generating far fields with tunable flat profiles," Opt. Lett. **37**, 2970–2972 (2012).

[63] Z. Mei and O. Korotkova, "Random sources generating ring-shaped beams," Opt. Lett. **38**, 91–93 (2013).

[64] Z. Mei and O. Korotkova, "Cosine-Gaussian Schell-model sources," Opt. Lett. **39**, 2578–2580 (2013).

[65] O. Korotkova, "Random sources for beams with rectangular symmetry," Opt. Lett. **39**, 64–67 (2013).

[66] O. Korotkova, "Random sources for beams with rectangular symmetry," Opt. Lett. **39**, 64–67 (2013).

[67] L. Ding, O. Korotkova, and L. Z. Pan, "The control of pulse profiles with tunable temporal coherence", Phys. Lett. A, **378**, 1687–1690 (2014).

[68] S. A. Ponomarenko, and E. Wolf, "Coherence properties of light in Young's interference pattern formed with partially coherent light," Opt. Commun., **170**, 1–8 (1999).

[69] M. Santarsiero, G. Piquero, J. C. G. de Sande, and F. Gori, "Difference of cross-spectral densities," Opt. Lett. **39**, 1713–1716 (2014).

[70] P. Vahimaa and J. Turinen, "Finite-elementary-source model for partially coherent radiation," Opt. Express **14**, 1376-1381 (2006).

[71] R. Martinez-Herrero, P. M. Mejias, and F. Gori, "Genuine cross-spectral densities and peudo-modal expansions," Opt. Lett. **34**, 1399-1401 (2009).

[72] S. A. Ponomarenko, G. P. Agrawal, and E. Wolf, "Energy spectrum of nonstationary ensemble of pulses," Opt. Lett. **29**, 394 (2004).

[73] S. A. Ponomarenko, H. Roychowdhury, and E. Wolf, "Physical Significance of Complete Spatial Coherence of Optical Fields," Phys. Lett. A, **345**, 10–12 (2005).

[74] J. Turunen and A. T. Friberg, "Propagation-Invariant Optical Fields," Progress in Optics, **54**, 1–88 (2010), ed. E. Wolf.

[75] S. A. Ponomarenko and G. P. Agrawal, "Linear optical bullets," Opt. Commun., **261**, 1–4 (2006).

[76] A. Starikov and E. Wolf, "Coherent-mode representation of Gaussian Schell-model sources and their radiation fields," J. Opt. Soc. Am. **72**, 923–928 (1982).

[77] C. Palma, R. Borghi, and C. Cincotti, "Beams originated by J_0-correlated Schell-model sources," Opt. Commun., **125**, 113–121 (1996).

[78] G. Zhou and X. Chu, "Propagation of partially coherent cosine-Gaussian beam through an ABCD optical system in turbulent atmosphere," Opt. Express **17** 10529–10534 (2009).

[79] L. Liu, "Partially coherent diffraction effect between Lau and Talbott effects," J. Opt. Soc. Am. A **5**, 1709–1716 (1988).

[80] A. W. Lohman and J. Ojeda-Castaneda, "Spatial periodicities in partially coherent fields," Opt. Acta: Int. J. Opt., **30**, 475–479 (1983).

[81] G. Indebetouw, "Propagation of spatially periodic wavefields," Opt. Acta:Int. J. Opt., **31**, 4–8 (1984).

[82] J. Turunen, A. Vasara, and A. T. Friberg, "Propagation invariance and self-imaging in variable-coherence optics," J. Opt. Soc. Am. A **8**, 282–289 (1991).

[83] S. Teng, L. Liu, J. Zu, Z. Luan, and L. Liu, "Uniform theory of the Talbott effect with partially coherent light illumination," J. Opt. Soc. Am. A **20**, 1747–1754 (2003).

[84] M Santarsiro, J. C. G. de Sande, G. Piquero, and F.Gori, "Coherence-polarization properties of fields radiated from transversely periodic electromagnetic sources," J. Opt., **15**, 055701 (2013).

[85] S. A. Ponomarenko, and E. Wolf, "The spectral degree of coherence of fully spatially coherent electromagnetic beams," Opt. Commun., **227**, 73–74 (2003).

Appendix A

Copyright Permission

From: Liyuan Ma[ly823106@dal.ca]
Sent: Tuesday, March 24, 2015 2:32 PM
To: pubscopyright[copyright@osa.org]

Dear Optical Society of America,
I am the first author of the following journals, while I was working towards my master degree. Now, I am preparing my master thesis for submission to the Faculty of Graduate Studies at Dalhousie University, Halifax, Nova Scotia, Canada. I'm seeking your permission to include a manuscript version of the following paper(s) as a chapter in the thesis:
1. Liyuan Ma and Sergey A. Ponomarenko, "Optical Coherence Gratings and Lattices," Optics Letters, Vol. 39, Issue 23, pp. 6656-6659 (2014).
2. Liyuan Ma and Sergey A. Ponomarenko, "Free-Space Propagation of Optical Coherence Lattices and Periodicity Reciprocity," Optics Express, Vol. 23, Issue 2, pp. 1848-1856 (2015).

Full publication details and a copy of this permission letter will be included in the thesis.

Regards
Liyuan Ma

From: pubscopyright [copyright@osa.org]
Sent: Monday March 30, 2015 12:42 PM
To: Liyuan Ma[ly823106@dal.ca]

Dear Liyuan Ma,
Thank you for contacting The Optical Society.
Because you are the author of the source paper from which you wish to reproduce material, OSA considers your requested use of its copyrighted materials to be permissible within the author rights granted in the Copyright Transfer Agreement submitted by the requester on acceptance for publication of his/her manuscript. It is requested that a complete citation of the original material be included in any publication. This permission assumes that the material was not reproduced from another source when published in the original publication.

Please let me know if you have any questions.

Kind Regards,
Susannah Lehman

Susannah Lehman
March 30, 2015
Authorized Agent, The Optical Society

Appendix B

Analytical Expression for Optical Coherence Lattice Pseudo-mode

The lattices pseudo-mode at the source plane can be expressed as

$$\psi_{\alpha_{n_s}}(s,0) = \frac{e^{-(\mathrm{Im}\,\alpha_{n_s})^2}}{\pi^{1/4}} \exp\left[-\frac{(s-\sqrt{2}\alpha_{n_s})^2}{2}\right]. \tag{B.1}$$

Here

$$\alpha_{n_s} = \frac{i\pi n_s}{a_s\sqrt{2}}, \tag{B.2}$$

where a_s is a (dimensionless) lattice constant in the s-direction and n_s is an integer.

Its Fourier(spectral) amplitude can be determined by the inverse Fourier transform,

$$\begin{aligned}\widetilde{\psi}(q,0) &= \int_{-\infty}^{+\infty} \frac{ds}{2\pi} e^{-iqs}\psi(s,0) \\ &= \frac{e^{-(\mathrm{Im}\,\alpha_{n_s})^2}}{\sqrt{2\pi}\pi^{1/4}} \exp\left[-\frac{q^2+2\sqrt{2}iq\alpha_{n_s}}{2}\right].\end{aligned} \tag{B.3}$$

Here, we used the standard Gaussian integral

$$\int_{-\infty}^{+\infty} dx e^{-ax^2+bx} = \sqrt{\frac{\pi}{a}} \exp\left[\frac{b^2}{4a}\right], \tag{B.4}$$

with $a = 1/2$ and $b = \sqrt{2}\alpha_{n_s} - iq$.

The optical lattices field propagation is governed by the paraxial wave equation in the form

$$2i\partial_Z\psi + \partial_s^2\psi = 0, \tag{B.5}$$

which can be converted to the $k-$space as

$$2i\partial_Z\widetilde{\psi} - q^2\widetilde{\psi} = 0. \tag{B.6}$$

Here the propagation distance Z is a dimensionless variable which is measured in Rayleigh range units z_R corresponding to a fully coherent source of the width σ_I,

$z_R = k\sigma_I^2$. Solving Eq (B.6),we can obtain

$$\begin{aligned} \widetilde{\psi}(q, Z) &= \widetilde{\psi}(q, 0) \exp\left[-\frac{iq^2 Z}{2}\right] \\ &= \frac{e^{-(\mathrm{Im}\,\alpha_{n_s})^2}}{\sqrt{2\pi}\pi^{1/4}} \exp\left[-\frac{(1+iZ)q^2 + 2\sqrt{2}iq\alpha_{n_s}}{2}\right]. \end{aligned} \tag{B.7}$$

Using the inverse Fourier transform, we obtain the expression for the lattice beam envelope at any distance Z as

$$\psi(s, Z) = \frac{e^{-(\mathrm{Im}\,\alpha_{n_s})^2}}{\pi^{1/4}(1+iZ)} \exp\left[-\frac{(s-\sqrt{2}\alpha_{n_s})^2}{2(1+iZ)}\right]. \tag{B.8}$$

Appendix C

Numerical Coding for Novel Optical Coherence Gratings and Lattices

```
**************************************************************************
**%%modulus of the temporal degree of
**%%coherence of the optical coherence grating
**************************************************************************
clc;
clear;
figure('numbertitle','off','color',[1,1,1]);
%%set parameters
x=0:0.01:10;  %%time difference
subplot(1,2,1);
N=2;
u1=sin(N.*x)./(N.*sin(x));
u=abs(u1);    %%mu
plot(x,u);
xlabel('$\frac{\pi}{2a}(T_2-T_1)$','interpreter','latex','fontsize',16);
ylabel('$|\gamma|$','interpreter','latex','fontsize',16);
subplot(1,2,2);
N=20;
u1=sin(N.*x)./(N.*sin(x));  % %mu
u=abs(u1);
plot(x,u);
xlabel('$\frac{\pi}{2a}(T_2-T_1)$','interpreter','latex','fontsize',16);

**************************************************************************
**%%Energy spectrum of the pulse with finite
**%%number N of equally weighted modes
**************************************************************************

**************************************************************************
```

```
clc;
clear;
figure('numbertitle','off','color',[1,1,1]);
% %set parameter
a=0.25; % %pulse period
N=20;%% case number
% % loop begin
u1=0;
x=0:0.01:100;
for i=1:N,
  u1=u1+exp(-(x-pi*i/a).^2);
end
plot(x,u1,'k');
xlabel('${\Omega}$','interpreter','latex','fontsize',16);
ylabel('energy spectrum','interpreter','latex','fontsize',16);
**********************************************************************
**% %magnitude of the spectral degree of coherence
**% %for a spatial coherence lattice
**********************************************************************
clear;
clc;
figure1=figure('numbertitle','off','color',[1,1,1]);
axes1=axes('Parent',figure1,'FontSize',18);
% %set parameter
N=20;
R=0.7;
xx=0:0.01:20;
yy=xx;
[x,y]=meshgrid(xx,yy);
u=abs(sin(N.*x)./(N.*sin(x)).*(sin(N.*R.*y)./(N.*sin(R.*y))));
surf(xx,yy,u);
shading interp;
xlabel('${\pi \over {2a_X}}(X_2 - X_1)$','interpreter','latex','fontsize
    ',20);
ylabel('${\pi \over {2a_Y}}(Y_2 - Y_1)$','interpreter','latex','fontsize
    ',20);
```

```
zlabel('${\mid \mu \mid}$','interpreter','latex','fontsize',20);
**********************************************************************
**%%the radiant intensity distribution of
**%%a spatial coherence lattice
**********************************************************************
clear;
clc;
figure('numbertitle','off','color',[1,1,1]);
% %set the parameter
N=20;
R=0,7;
xx=0:0.05:20;
yy=0:0.05:20;
[x,y]=meshgrid(xx,yy);
i=1;
j=1;
a=0.5;
b=a/R;
u1=0;
u2=0;
for i=1:N
  for j=1:N
    u2=u2+exp(-(y-pi.*i./b).^2);
    j=j+1;
  end
u1=u1+exp(-(x-pi.*i./a).^2);
i=i+1;
end
u=u1+u2;
surf(xx,yy,u);
shading interp;
xlabel('${\pi \over {2a_x}}(x_2 - x_1)$','interpreter','latex','fontsize
    ',20);
ylabel('${\pi \over {2a_y}}(y_2 - y_1)$','interpreter','latex','fontsize
    ',20);
zlabel('Intensity','interpreter','latex','fontsize',20);
```

Appendix D

Numerical Coding for Optical Lattices Beams Propagate in Free-Space

```
**********************************************************************
**% %the intensity profile of a uniformly distributed optical
**% %coherent lattices for different distance
**********************************************************************
clear;
clc;
% % set parameter
figure('numbertitle','off','color',[1,1,1])
vx=1;%v_x
vy=1;%v_y
ax=1;%a_x
R=1;
ay=ax.*R;%a_y
N=10;%n_x &n_y
subplot(3,2,1,'FontSize',14);
z=0;
u1=0;
u2=0;
xx=-5:0.1:5;
yy=-5:0.1:5;
[x,y]=meshgrid(xx,yy);
% %begin the loop
for i=1:N
  for j=1:N
    u2=u2+exp(-((y-pi.*j.*z./ay).^2)./(1+z.^2))./(pi.*(1+z.^2));
  end
u1=u1+exp(-((x-pi.*i.*z/ax).^2)./(1+z.^2))./(pi.*(1+z.^2));
end
```

```
************************************************


% % get the intensity
I=u1.*u2;
surf(xx,yy,I);
shading interp;
xlabel('X',...
'interpreter','latex','fontsize',24);
text(0.5,9,'z=0','fontsize',14);
ylabel('Y',...
'interpreter','latex','fontsize',24);
zlabel('Intensity',...
'interpreter','latex','fontsize',24);
view(20,40)
% %second plot
subplot(1,2,2,'FontSize',14);
z=0.3;
u1=0;
u2=0;
xx=-5:0.05:15;
yy=-5:0.05:15;
[x,y]=meshgrid(xx,yy);
for i=1:N
for j=1:N
u2=u2+exp(-((y-pi.*j.*z./ay).^2)./(1+z.^2))./(pi.*(1+z.^2));
end
u1=u1+exp(-((x-pi.*i.*z/ax).^2)./(1+z.^2))./(pi.*(1+z.^2));
end
% % get the intensity
I=u1.*u2;
surf(xx,yy,I);
shading interp;
xlabel('X','interpreter','latex','fontsize',24);
text(-10,30,'z=0.3','fontsize',14);
ylabel('Y','interpreter','latex','fontsize',24);
zlabel('Intensity','interpreter','latex','fontsize',24);
view(20,40)
************************************************************
```

```
**% %the spectral degree of coherence of a uniformly distributed
**% %optical coherent lattices for several propagation distance
************************************************************
clear;
clc;
figure('numbertitle','off','color',[1,1,1])
N=10;
v_s=1;
ax=1;
R=1;
ay=ax*R;
i=(-1).^0.5;
x1=0;
y1=0;
% %seting the parameter
subplot(1,2,1,'FontSize',14);
z=0;
xx=-5:0.01:5;
yy=-5:0.01:5;
[x,y]=meshgrid(xx,yy);
% %get W
Wy=0;
Wx=0;
for j=1:N
Wy=Wy+exp(i.*(y1.^2-y.^2)./(2.*(z+1./z))).*exp(i.*pi.*j.*(y1-y)./(ay
    .*(1+z.^2))).*exp(-((y1-(pi.*j.*z./ay)).^2+(y-(pi.*j.*z./ay)).^2)
    ./(2.*(1+z.^2))).//((pi.*(1+z.^2)).^0.5);%phase is (exp(i.*(y1.^2-y
    .^2)./(2.*(z+1./z))).//(pi.*(1+z.*2)).^0.5).*exp((i.*pi.*j.*(y-y1))
    .//((1+z.^2).*ay)).*
end
for k=1:N
Wx=Wx+exp(i.*(x1.^2-x.^2)./(2.*(z+1./z))).*exp(i.*pi.*k.*(x1-x)./(ax
    .*(1+z.^2))).*exp(-((x1-(pi.*k.*z./ax)).^2+(x-(pi.*k.*z./ax)).^2)
    ./(2.*(1+z.^2))).//((pi.*(1+z.^2)).^0.5);%phase is (exp(i.*(x1.^2-x
    .^2)./(2.*(z+1./z))).//(pi.*(1+z.*2)).^0.5).*exp((i.*pi.*k.*(x-x1))
    .//((1+z.^2).*ax)).*
end
W=Wx.*Wy;
% % get I1
```

```
u1=0;
u2=0;
for j=1:N
u2=u2+exp(-((y1-pi.*j.*z./ay).^2)./(1+z.^2));
end
for k=1:N
u1=u1+exp(-((x1-pi.*k.*z/ax).^2)./(1+z.^2));
end
I1=u1.*u2./(pi.*(1+z.^2));
% % get I2
u1=0;
u2=0;
for j=1:N
u2=u2+exp(-((y-pi.*j.*z./ay).^2)./(1+z.^2));
end
for k=1:N
u1=u1+exp(-((x-pi.*k.*z/ax).^2)./(1+z.^2));
end
I2=u2.*u1./(pi.*(1+z.^2));
% % plot the u
u=W./(((I1).^0.5).*((I2).^0.5));
U=abs(u);
surf(x,y,U);
shading interp;
xlabel('X','interpreter','latex','fontsize',24);
text(-10,10,'z=0','fontsize',14);
ylabel('Y','interpreter','latex','fontsize',24);
zlabel('${\mid \mu \mid}$','interpreter','latex','fontsize',24);
view(20,40)
% % second plot
subplot(1,2,2,'FontSize',14);
z=0.1; % % distance
x1=0;
y1=0;
xx=-10:0.1:10;
yy=-10:0.1:10;
[x,y]=meshgrid(xx,yy);
i=(-1).^0.5;
% % get W
```

```
Wy=0;
Wx=0;
for j=1:N
Wy=Wy+exp(i.*(y1.^2-y.^2)./(2.*(z+1./z))).*exp(i.*pi.*j.*(y1-y)./(ay
    .*(1+z.^2))).*exp(-((y1-(pi.*j.*z./ay)).^2+(y-(pi.*j.*z./ay)).^2)
    ./(2.*(1+z.^2))).//((pi.*(1+z.^2)).^0.5);% %phase is (exp(i.*(y1.^2-y
    .^2)./(2.*(z+1./z))).//(pi.*(1+z.*2)).^0.5).*exp((i.*pi.*j.*(y-y1))
    .//((1+z.^2).*ay)).*
end
for k=1:N
Wx=Wx+exp(i.*(x1.^2-x.^2)./(2.*(z+1./z))).*exp(i.*pi.*k.*(x1-x)./(ax
    .*(1+z.^2))).*exp(-((x1-(pi.*k.*z./ax)).^2+(x-(pi.*k.*z./ax)).^2)
    ./(2.*(1+z.^2))).//((pi.*(1+z.^2)).^0.5);% % phase is (exp(i.*(x1.^2-
    x.^2)./(2.*(z+1./z))).//(pi.*(1+z.*2)).^0.5).*exp((i.*pi.*k.*(x-x1))
    .//((1+z.^2).*ax)).*
end
W=Wx.*Wy;
% % get I1
u1=0;
u2=0;
for j=1:N
u2=u2+exp(-((y1-pi.*j.*z./ay).^2)./(1+z.^2));
end
for k=1:N
u1=u1+exp(-((x1-pi.*k.*z/ax).^2)./(1+z.^2));
end
I1=u1.*u2./(pi.*(1+z.^2));
% % get I2
u1=0;
u2=0;
for j=1:N
u2=u2+exp(-((y-pi.*j.*z./ay).^2)./(1+z.^2));
end
for k=1:N
u1=u1+exp(-((x-pi.*k.*z/ax).^2)./(1+z.^2));
end
I2=u2.*u1./(pi.*(1+z.^2));
% % plot the u
u=W./(((I1).^0.5).*((I2).^0.5));
```

```
U=abs(u);
surf(x,y,U);
shading interp;
xlabel('X','interpreter','latex','fontsize',24);
text(-5,20,'z=0.1','fontsize',14);
ylabel('Y','interpreter','latex','fontsize',24);
zlabel('${\mid \mu \mid}$','interpreter','latex','fontsize',24);
view(20,40)
```